A model for episodic degassing of an andesitic magma intrusion

Marie Boichu,[1,2] Benoît Villemant,[1,3] and Georges Boudon[1]

Received 23 April 2007; revised 9 February 2008; accepted 12 March 2008; published 9 July 2008.

[1] Episodic magmatic degassing has been observed at numerous volcanoes, especially those of intermediate composition. It can span timescales from years to decades. Here we propose a physical model for the degassing of a shallow magma intrusion to explain this phenomenon. The magma cools by convection, which leads to melt crystallization, volatile exsolution, and magma overpressure. When the pressure reaches a critical value, wall rocks fracture and the exsolved gas escapes. The intrusion then returns to the initial lithostatic pressure and a new cooling-crystallization-degassing cycle occurs. A series of such cycles leads to episodic degassing. The trend and timescale of the degassing process are mainly governed by magma cooling. Two degassing regimes are exhibited: an early phase with a high frequency of gas pulses and a later phase with a lower gas pulse frequency. The transition between these two regimes is caused by the viscosity increase when the magma crystallinity exceeds the crystal percolation threshold. We find that the time to this transition is dependent on magma volume, to a first approximation. Where observations are available from sustained geochemical surveillance, the model provides constraints on key aspects of the subsurface magmatic system, with estimation of the volume of an intrusion and tensile strength of the surrounding rocks. It therefore represents a relevant tool for volcanic surveillance and hazard assessment.

Citation: Boichu, M., B. Villemant, and G. Boudon (2008), A model for episodic degassing of an andesitic magma intrusion, *J. Geophys. Res.*, *113*, B07202, doi:10.1029/2007JB005130.

1. Introduction

[2] Noneruptive episodic degassing is a common feature at many intermediate to silicic volcanoes worldwide. Such degassing is typically sustained for years to decades, with nonrandom, short-duration gas "crises" superimposed on a longer-term secular degassing trend. Volcanoes where such behavior has been observed include La Soufrière de Guadeloupe (Lesser Antilles, France) [*Villemant et al.*, 2005], Campi Flegrei (Italy) [*Chiodini et al.*, 2003], Galeras (Colombia) [*Fischer et al.*, 1996], Vulcano Island (Italy) [*Nuccio and Paonita*, 2001], Poás (Costa Rica) [*Rowe et al.*, 1992], White Island (New Zealand) [*Giggenbach and Sheppard*, 1989] (Figure 1). The mechanism of magma convection in a conduit has been proposed to explain long-term regular and intense degassing of volatiles from andesitic magma chambers [*Stevenson and Blake*, 1998; *Shinohara et al.*, 2002; *Kazahaya et al.*, 2002]. Moreover, different processes suggested in literature could explain fluctuations of the gas flux or composition measured either in plumes, fumaroles or in thermal springs. A series of distinct degassing events may be generated by magma rise at shallow depth in discontinuous separate events [*Nuccio and Paonita*, 2001]. Enhanced by the heat dissipated from a close magma, processes of hydrofracturing [*Rowe et al.*, 1992], thermal cracking or sealing [*Edmonds et al.*, 2003] have been proposed to explain episodic release or trapping of magmatic fluids. During gas transfer to the surface, variations of the permeability of the hydrothermal system, often due to surficial sealing processes, may occur [*Zlotnicki et al.*, 1992; *Fischer et al.*, 1994; *Harris and Maciejewski*, 2000]. Thermochemical models show that decompression, cooling, oxidation processes, interactions with wall rocks and with the hydrothermal system, may lead to large variations in the volatile proportions in volcanic plumes [*Giggenbach and Sheppard*, 1989; *Symonds et al.*, 2001]. Eventually, the proportion of volatile components in surface waters may be modified by the dynamics of the aquifers varying due to external influences, such as the seasonal supply of meteoric waters [e.g., *Ingebritsen et al.*, 2001; *López et al.*, 2006]. Most of these mechanisms explain the observation of intermittent gas fluctuations but not their nonrandom repetition over a long time interval. This may be directly linked to a magmatic source that expels its fluids episodically.

[3] As an example, La Soufrière de Guadeloupe underwent an important volcanic crisis in 1975–1977 with many phreatic explosions [*Feuillard et al.*, 1983; *Komorowski et al.*, 2005]. Since then, thermal springs have been sampled about twice a month and show a pattern of episodically

[1]Institut de Physique du Globe de Paris, Équipe de Géologie des Systèmes Volcaniques, Paris, France.
[2]Now at Department of Geography, University of Cambridge, Cambridge, UK.
[3]Université Pierre et Marie Curie, Paris, France.

Copyright 2008 by the American Geophysical Union.
0148-0227/08/2007JB005130$09.00

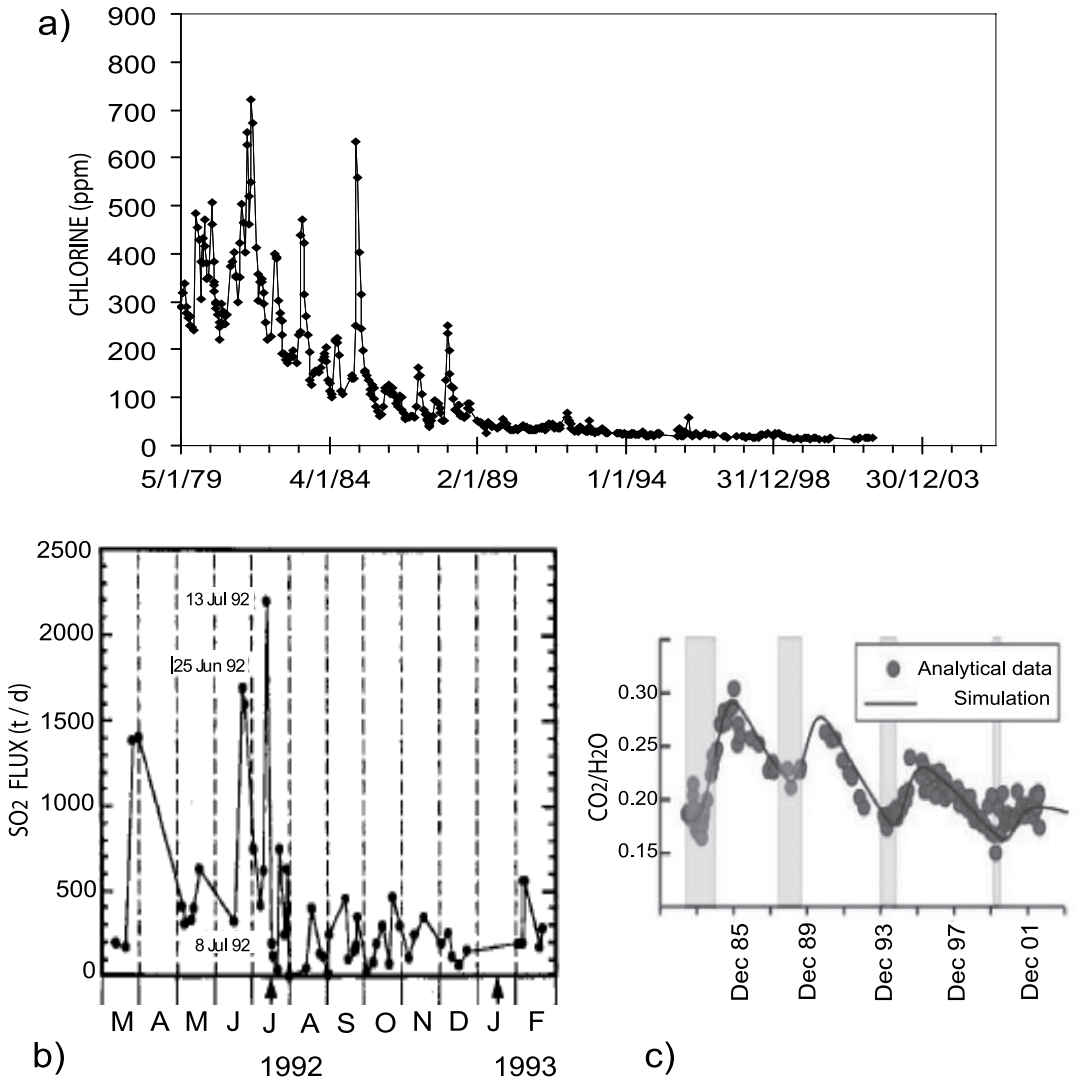


Figure 1. Episodic degassing observed at (a) La Soufrière de Guadeloupe (Lesser Antilles, France) through the temporal variations in the chlorine content sampled at Carbet Echelle thermal spring over a period of ~12 years (reproduced from *Villemant et al.* [2005]), (b) Galeras (Colombia) through the time variation in SO_2 flux (metric tons per day, m d^{-1}) remotely measured by COSPEC between the eruptions of 16 July 1992 and 14 January 1993 (reproduced from *Fischer et al.* [1996]), (c) Campi Flegrei (Italy) through the temporal variations in the gas composition expressed as CO_2/H_2O (molar ratio) from 1981 until 2002 (reproduced from *Chiodini et al.* [2003]).

changing hydrothermal fluid compositions (Figure 1a). Such a sustained monitoring data set is rare for a nonerupting volcano. The phreatic crisis, the subsequent evolution of the thermal spring compositions, and the accompanying shallow seismicity have all been interpreted as the consequences of a shallow magma intrusion [*Villemant et al.*, 2005].

[4] Our aim here is to develop a general model that describes the episodic degassing of a shallow intrusion of andesitic magma. If a volcano acts as a closed system, with no recharge or loss of magma by eruption, and exhibits an episodic degassing behavior, it may be the signature of a degassing stored magma. In this case, the interpretation of real geochemical data with the model would provide information on this subsurface magmatic system. When a magma body stalls in the crust, as it loses heat to the host rocks, it cools and crystallizes. This leads to the oversaturation of dissolved volatiles, which then exsolve and pressurize the magma intrusion [*Blake*, 1984; *Tait et al.*, 1989]. The generated overpressure may exceed a threshold that induces wall rock failure. The high viscosity of highly crystalline andesitic magmas inhibits dike propagation into the opened fractures [*Marsh*, 1981; *Rubin*, 1995a, 1995b] and instead decompression can occur through gas escape. Then, the intrusion returns to its original pressure and a new cycle of cooling-crystallization-degassing occurs leading to episodic degassing. Gases rise rapidly to the surface forming fumaroles, plumes, or interacting with the surficial hydrothermal system. The model therefore considers three main processes: the mechanisms of magma cooling and crystallization, the magma pressurization induced by melt crystallization and the process of episodic gas expulsion. The influence of the initial conditions of the magma intrusion on the different

regimes of magma degassing is discussed. This allows the characterization of the initial conditions that play a key role in the degassing and the physical mechanisms by which they exert this strong influence. Observations of fossil intrusions [*Marsh*, 2000; *White and Herrington*, 2000] and of persistent degassing activities [*Francis et al.*, 1993; *Allard*, 1997] support the idea that magma frequently does not reach the surface. It may stall at shallow depth in the crust and perturb volcanic and hydrothermal activity, both on short timescales with phreatic or phreatomagmatic eruptions, but also on decadal timescales by sustained fumarolic degassing. This model is consequently of particular relevance for volcano monitoring and hazard assessment purposes.

2. Model Description

[5] Our model describes the degassing of an andesitic magma following its intrusion at shallow depth. It is based on the following assumptions. Magma is a typical water-rich silicic andesite consisting of a rhyolitic melt (with 3 to 6 wt % H_2O) with a significant quantity of crystals. Magma is stored at a depth where it is volatile saturated. It has already lost some gas exsolved during its ascent. The magma intrusion, assumed spherical, evolves as a closed system. Because of the thermal contrast with the surroundings, the magma convects to transfer heat to the country rock where it is then assumed to be diffused by conduction. In the reservoir interior, only the process of thermal convection is considered; compositional convection and crystal settling are neglected [*Martin and Nokes*, 1989]. Magma cooling leads to melt crystallization, water exsolution and magma overpressure. An elastic homogeneous enclosing medium is considered. When the overpressure reaches a specific threshold, assumed constant with time, wall rocks fracture and the excess gas escapes instantaneously from the intrusion. After the gas expulsion, pressure returns to lithostatic, the system is closed again and a new cooling-crystallization-degassing cycle occurs. A series of such cycles leads to episodic degassing process. The model describes the degassing until the magma no longer convects. This mechanism has a short timescale with respect to the time of complete magma cooling. The global model may be divided in three stages: (1) magma cooling and crystallization, (2) magma pressurization induced by melt crystallization, and (3) episodic gas expulsion. In the following sections, we develop the theoretical framework of the model and provide the expressions of the model outputs that may be compared with geochemical monitoring data. Finally, we estimate the realistic range of model input values. Figure 2 summarizes the physical processes involved in magma degassing, the observable model outputs, the main variables and the model inputs. All symbols, notations and indices used are defined in Tables 1 and 2. Model inputs, variables, and outputs are listed in Table 3. The set of fixed physical parameters is given in Table 4.

2.1. Magma Crystallization, Cooling, and Viscosity Evolution

[6] The processes of magma cooling and crystallization are described via the spatially averaged magma temperature and mass of crystals. A simplified model (Figure 2, step 1) is built with the following assumptions. Magma undergoes thermal convection. Heat transfers to the surroundings are approximated by the simple case of a magma which cools due to contact with a cold vertical semi-infinite flat plate held at constant temperature. Heat loss is balanced by the variation of the magma temperature and the latent heat of crystallization. The evolution of the mean magma temperature with time can be formulated as follows [*Spera*, 1980]:

$$\frac{dT}{dt} = -\frac{\frac{3a_{\mathrm{th}}}{R^{2-3b_{\mathrm{th}}}}\left(\frac{\alpha_{\mathrm{th}} g}{\nu}\right) b_{\mathrm{th}} K_{\mathrm{th}}^{1-b_{\mathrm{th}}} \left(T - T_{\mathrm{contact}}\right)^{1+b_{\mathrm{th}}}}{1 + \frac{L}{C_p (T_l - T_s)}}. \qquad (1)$$

Both coefficients a_{th} and b_{th} depend on the type of heat transfer. We assume that the andesitic magmas are highly crystalline and viscous such that convection is laminar and b_{th} is $\sim$0.25 [*Bejan*, 1984]; a_{th} also depends on magma geometry and is $\sim$0.7 [*Churchill and Usagi*, 1972].

[7] A simple dependency of crystallization on the temperature decrease is assumed:

$$\frac{1}{M}\frac{dm_c}{dt} = -\frac{1}{(T_l - T_s)}\frac{dT}{dt}. \qquad (2)$$

Relation (2) is classically used for $T_s < T < T_l$, with a crystal mass equal to zero at the liquidus temperature. Andesites contain a fraction of inherited crystals and the crystal mass is consequently not necessarily zero at $T = T_l$. Thus, initial magma temperature and crystallinity are independent conditions.

[8] The contact temperature is approximated by that obtained with models which describe both magma cooling and host rock heating by conductive heat transfer [*Carslaw and Jaeger*, 1986], assuming no hydrothermal convection in the surroundings. For similar thermal diffusivity of magma and wall rocks, T_{contact} may be considered constant and, to a first approximation, given by

$$T_{\mathrm{contact}} = \frac{1}{2}\left(T_i + T_{\mathrm{surroundings}}\right) = \frac{1}{2}(2T_i - \Delta T). \qquad (3)$$

Relation (3) is valid while $t < 0.4\, R^2/K_{\mathrm{th}}$, a condition always met in our study of the first stages of the cooling process.

[9] According to equation (1), and because it may vary significantly in crystallizing andesitic magmas, magma viscosity plays a key role in cooling. It is controlled by numerous variables, which may be dependent, including magma crystallinity, crystal sizes and shapes, magma composition and temperature, and water content of melt and bubbles. When the crystal fraction Φ exceeds the percolation threshold of the solid particles Φ_P of the order of 40 vol % [*Rutgers*, 1962; *Shaw*, 1969; *Wildemuth and Williams*, 1985; *Ryerson et al.*, 1988; *Lejeune and Richet*, 1995], the viscosity may increase dramatically, by 5–6 orders of magnitude as Φ changes from 40 to 60% [*Lejeune and Richet*, 1995] (see Appendix A, Figure A1). Crystal content of silicic andesitic magmas is typically within the range 25–50 vol %, thus we assume that it is the primary control of magma viscosity.

[10] A rapid review of the role of the other variables is presented below and shows that they imply second-order

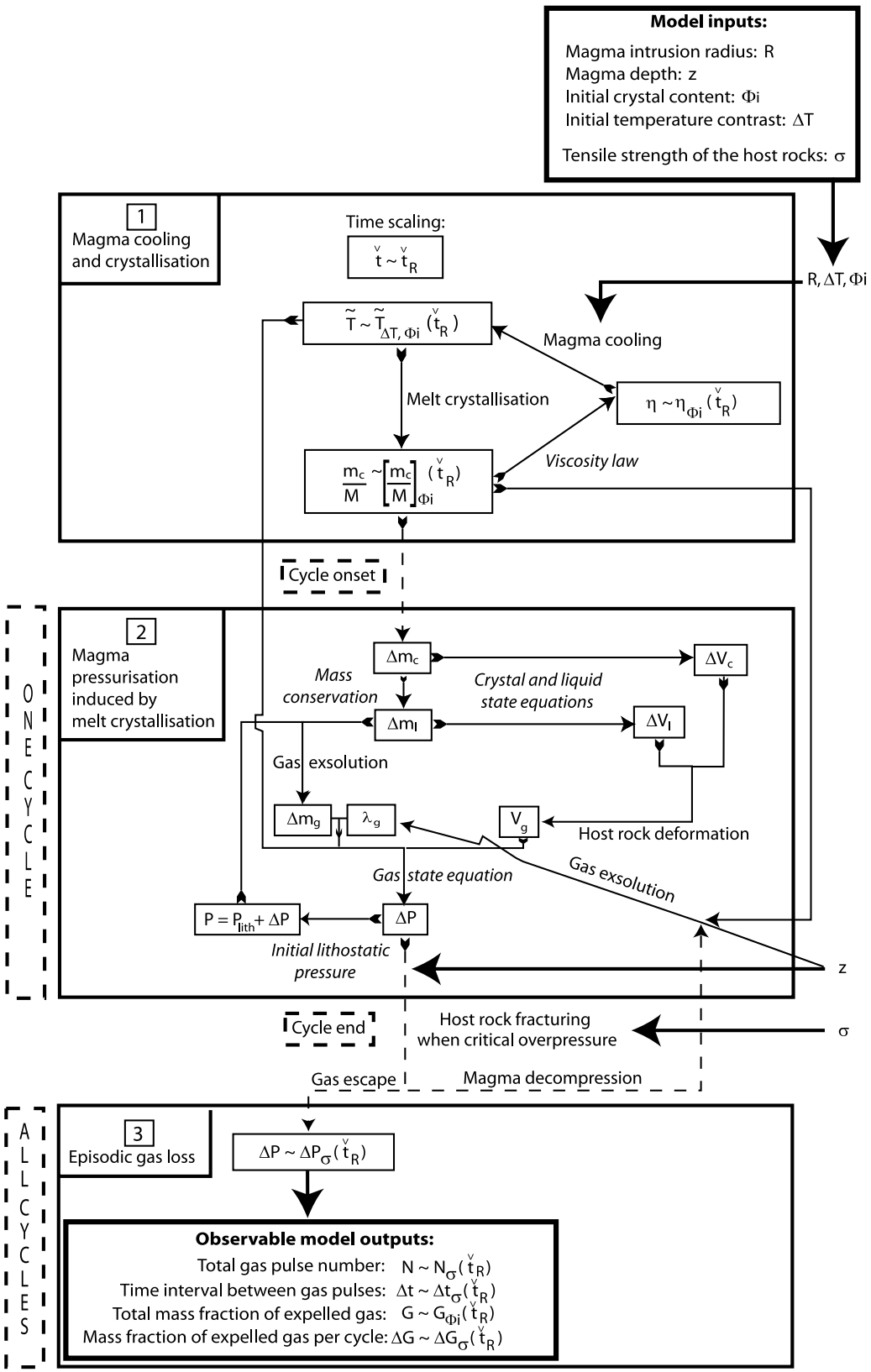


Figure 2. Schematic description of the three steps of the model: (1) magma cooling and crystallization, (2) magma pressurization induced by melt crystallization, and (3) episodic gas expulsion. The physical processes taken into account and the involved model outputs, inputs and variables are detailed. The dependence relationships obtained (section 3) between the model outputs and relevant variables, and the model inputs are mentioned. The cyclic evolution is underlined with dashed lines. All used symbols are listed in Tables 1 and 2.

Table 1. Latin Symbols Used[a]

Symbol	Definition
a_{th}	thermal transfer coefficient
A	ratio of the perfect gas constant to the molar mass of the volatile species, J kg^{-1} K^{-1}
A_{incl}	inclination of the parallel asymptotes of the viscosity curve
b_{th}	thermal transfer coefficient
B_{asympt}	distance between the asymptotes of the viscosity curve
C_{slope}	slope at the inflexion point of the viscosity curve
C_P	silicate melt heat capacity, J kg^{-1} K^{-1}
g	acceleration due to gravity, m^2 s^{-1}
k	cooling-crystallization-degassing cycle number
K_{th}	silicate melt thermal diffusivity, m^2 s^{-1}
L	magma crystallization latent heat, J kg^{-1}
m	mass, kg
G	total mass fraction of expelled gas with the initial available mass of gas just after intrusion
M	total mass of magma, kg
n	exponent of the water solubility law written $x = sP^n$
n_R	exponent of the Roscoe law
N	gas pulse number since magma intrusion
P	magma pressure, Pa
R	magma intrusion radius, m
s	water solubility coefficient
t	time, s
$\tilde{t}$	dimensionless time
$\breve{t}$	rescaled time relative to the time until convection ceases
t_{conv}	time to cessation of convection, s
t_C	time to the transition in the cooling process, s
t_D	time to the transition in the degassing process, s
T	average magma temperature, K
$T_{contact}$	contact temperature between magma and surroundings, K
$T_{surroundings}$	temperature of the surrounding rocks, K
T_i	initial magma temperature just after intrusion, K
T_l	magma liquidus temperature, K
T_s	magma solidus temperature, K
x	weight fraction of the volatile species dissolved in the melt m_d/m_l
z	magma intrusion depth, m

[a]Subscript k refers to the initial variables values for a given cycle k, and any variable topped by an overbar refers to the final variable value, just before fracturing. Subscript i refers to the initial variables values just after intrusion. Any variable topped by a tilde refers to the dimensionless variable.

Table 2. Greek Symbols Used[a]

Symbol	Definiton
α_{th}	silicate melt thermal expansion, K^{-1}
β_{liq}	bulk modulus of silicate liquid, Pa
η	magma dynamic viscosity, Pa s
η_0	dynamic viscosity of the homogeneous magmatic liquid, Pa s
η_{inflex}	dynamic viscosity at the inflexion point of the viscosity curve, Pa s
Φ	crystal volume fraction, vol %
Φ_i	initial volume fraction of crystals, vol %
Φ_{inflex}	crystal volume fraction at the inflexion point of the viscosity curve, vol %
Φ_m	crystal volume fraction preventing any liquid movement, vol %
Φ_P	volume fraction of crystals at their percolation threshold, vol %
λ_g	fraction of exsolved gas mass at cycle onset with the total mass of magma (m_g/M)
μ	rigidity of the surrounding rocks, Pa
$\bar{\mu}$	4/3 times the host rock rigidity, Pa
ν	magma kinematic viscosity, m^2 s^{-1}
ρ	magma density, kg m^{-3}
ρ_{litho}	lithostatic density, kg m^{-3}
σ_t	tensile strength of the surrounding rocks, Pa
τ	characteristic time of magma cooling, s
$\Delta_k(m)$	increase of mass during a given cycle k, kg
ΔP	magma overpressure, Pa
Δt	time interval between two consecutive gas pulses, s
ΔG	fraction of expelled gas mass per pulse with the initial available mass of gas just after intrusion
ΔT	initial temperature contrast between magma and surroundings, K

[a]Subscripts l, c, g, d refer to the liquid, crystal, and exsolved and dissolved gas phases, respectively. Subscript k refers to the initial variables values for a given cycle k, and any variable topped by an overbar refers to the final variable value, just before fracturing. Subscript i refers to the initial variables values just after intrusion. Any variable topped by a tilde refers to the dimensionless variable.

variations on viscosity. The percolation threshold lowers with decreasing solid particles sizes [*Ward and Whitmore*, 1950a, 1950b] and symmetry [*Milliken et al.*, 1989]. However, these effects are minor compared to the role of the crystal fraction [*Lejeune and Richet*, 1995]. The cooling of a rhyolitic melt by 200°C from an initial temperature of ~950°C, typically produces an increase of the viscosity of 2–3 orders of magnitude [*Neuville et al.*, 1993; *Hess and Dingwell*, 1996]. Melt crystallization also implies changes in melt composition manifested in an increase in silica content and consequently in melt polymerization and viscosity. Such well-known effects are of limited impact in this case. Isobaric cooling, crystallization and degassing lead to negligible variations in dissolved water contents (<0.1 wt %) and melt viscosity [*Hess and Dingwell*, 1996; *Richet et al.*, 1996; *Stevenson et al.*, 1998]. The presence of gas bubbles implies a viscosity decrease but in a limited range if bubble fraction is 40 vol % [*Lejeune*, 1994]. This is the case in our model where exsolved gas periodically escapes from the magma. The combined influence of these different variables is poorly known. Since the temperature decrease and the melt polymerization both increase the viscosity, assuming a rheology only dependent on the crystal fraction underestimates the viscosity variations with time. The proposed analytical viscosity law and the method to determine it are given in Appendix A.

Table 3. Model Inputs, Relevant Variables, and Outputs[a]

Model Inputs	Symbol	Range (Reference Value)
Initial conditions of magma intrusion		
Initial crystal volume fraction (vol %)	Φ_i	30–50 (40)
Magma intrusion radius (m)	R	5–500 (200)
Initial temperature contrast between magma and surroundings (K)	ΔT	200–800 (400)
Magma intrusion depth (m)	z	[2–10] (3) × 10^3
Initial condition of host rocks		
Tensile strength of the host rocks (Pa)	σ_t	[0.01–10] (1) × 10^6
Relevant model variables		
Magma temperature	T	
Magma dynamic viscosity	η	
Magma crystal content	m_c/M	
Magma overpressure	ΔP	
Model outputs		
Time interval between two consecutive pulses	Δt	
Gas pulse number since magma intrusion	N	
Mass fraction of expelled gas per pulse	ΔG	
Total mass fraction of expelled gas since magma intrusion	G	

[a]See section 2.5 for further explanations of model inputs.

Table 4. Fixed Model Physical Parameters

Model Physical Parameters	Symbol	Value	Source
Characterizing Magma Intrusion			
Silicate melt thermal expansion (K^{-1})	α_{th}	5×10^{-5}	
Inclination of the parallel asymptotes of the viscosity curve	A_{rot}	2.4	see Appendix A
Bulk modulus of silicate liquids (Pa)	β_{liq}	10^{10}	*Touloukian et al.* [1981]
Distance between viscosity law asymptotes	B_{asympt}	1.5	see Appendix A
Slope at the inflexion point of the viscosity curve	C_{slope}	80.0	see Appendix A
Silicate melt specific heat (J kg^{-1} K^{-1})	C_P	1000	*Richet and Bottinga* [1986]
Crystal volume fraction at the inflexion point of the viscosity curve (vol %)	Φ_{inflex}	0.5	see Appendix A
Silicate melt thermal diffusivity (m^2 s^{-1})	K_{th}	10^{-6}	*Bagdassarov et al.* [1996]
Melt crystallization latent heat (J kg^{-1})	L	3.3×10^5	*Nicholls and Stout* [1982]
Solubility law exponent	n	0.5	*Burnham* [1975]
Magma dynamic viscosity at the inflexion point of the viscosity curve (Pa s)	η_{inflex}	10^{11}	see Appendix A
Crystal density (kg m^{-3})	ρ_c	3100	
Silicate liquid density (kg m^{-3})	ρ_l	2400	*Spera* [2000]
Solubility law coefficient ($Pa^{-1/2}$)	s	4.11×10^{-6}	*Burnham* [1962]
Initial magma temperature just after intrusion (K)	T_i	1173	*Scaillet and Pichavant* [2003]
Magma liquidus temperature (K)	T_l	1223	*Spera* [2000]
Magma solidus temperature (K)	T_s	1023	*Spera* [2000]
Independent of Magma Intrusion			
Thermal transfer coefficient	a_{th}	0.67	*Churchill and Usagi* [1972]
Thermal transfer coefficient	b_{th}	0.25	*Bejan* [1984]
Crystal volume fraction preventing any liquid movement (vol %)	Φ_m	0.6	see Appendix A
Crystal percolation threshold (vol %)	Φ_P	0.4	see section 2.1
Rigidity of surrounding rocks (Pa)	μ	10^{10}	*Touloukian et al.* [1981]
Roscoe law coefficient	n_R	2.5	see Appendix A
Lithostatic density (kg m^{-3})	ρ_{litho}	2400	

[11] The magma cooling law (equation (1)) may be written in a nondimensional form:

$$\frac{d\tilde{T}}{d\tilde{t}} = \frac{\nu(\Phi_i)}{\nu\left(\Phi\left(\tilde{T}\Delta T + T_i\right)\right)}\left(\tilde{T} + \frac{1}{2}\right)^{1+b_{th}}, \tag{4}$$

with $\tilde{T} = (T - T_i)/\Delta T$ and $\tilde{t} = t/\tau$. The characteristic time τ, which depends on the initial conditions (R, ΔT, Φ_i), is defined by

$$\tau(R, \Delta T, \Phi_i) = \frac{1 + \frac{L}{C_p(T_l - T_s)}}{\frac{3a_{th}}{R^{2-3b_{th}}}\left(\frac{\alpha_{th} g}{\nu(\Phi_i)}\right)^{b_{th}} K_{th}^{1-b_{th}} \Delta T^{b_{th}}}. \tag{5}$$

Equation (4) is numerically solved using a Runge-Kutta method, from $t = 0$ corresponding to magma intrusion until magma crystallinity reaches 60 vol %. Beyond this value, magma behaves as a solid [*Lejeune and Richet*, 1995]. We restrict the model to the convective cooling regime.

2.2. Magma Pressurization Induced by Melt Crystallization

[12] Magma is composed of three phases: crystal, liquid, and gas. It is in thermodynamic equilibrium, and all system variables are assumed homogeneous. *Tait et al.* [1989] expressed the magma pressure as a function of its crystallization taking into account the effects of the initial pressure, via the solubility law of volatiles in the melt, the deformation of the surrounding rocks assumed elastic, the initial mass of exsolved gas and the crystallization-induced contraction of the magma. Here, we extend this model by imposing an initial crystal content. In addition, we consider a cyclic host rock fracturing and gas escape. A schematic illustration of the model is given in (Figure 2, step 2). For a given cycle k, this leads to the equation of state for magma

$$f_k(P, T) = \frac{\Delta_k(m_c)}{M} \tag{6}$$

with

$$f_k(P,T) = \frac{\left[1 - \left(\frac{P_k}{P}\right)^n\right]\left(1 - \frac{m_{ck}}{M}\right) + \left(\frac{P}{P_k} - 1\right)\left[\frac{PP_k}{AT_{\rho_l} sP^n}\left(\frac{1}{\mu} + \frac{1}{\beta_{liq}}\right)\left(1 - \frac{m_{ck}}{M}\right) + \frac{PP_k}{AT_{\rho_c} sP^n}\frac{1}{\mu}\frac{m_{ck}}{M} + \frac{\lambda_{gk}}{sP^n}\right]}{1 + \frac{1}{sP^n}\frac{P}{AT}\left(\frac{1}{\rho_c} - \frac{1}{\rho_l}\right)} = \frac{N_1 + N_2}{1 + \frac{1}{sP^n}\frac{P}{AT}\left(\frac{1}{\rho_c} - \frac{1}{\rho_l}\right)}. \tag{7}$$

The denominator in equation (7) describes the magma contraction due to melt crystallization. N_1 is rewritten

$$N_1 \approx \left[1 - \left(\frac{P_k}{P}\right)^n\right] \frac{m_{lk}}{M}, \tag{8}$$

with $m_{lk}/M = (1 - (m_{ck}/M))$ for mass conservation, where the mass of gas is neglected relative to the masses of liquid and crystals. It describes the contribution of gas exsolution which results from the combined influence of the mass of residual melt and of the initial pressure via the water solubility law. Assuming the ideal gas law $\rho_g = P/AT$, the second term is rewritten

$$\begin{aligned} N_2 &= \frac{P - P_k}{x}\left(N_{2l} + N_{2c} + N_{2g}\right) \\ &= \frac{P - P_k}{x}\left[\left(\frac{1}{\mu} + \frac{1}{\beta_{\text{liq}}}\right)\frac{\rho_g}{\rho_l}\frac{m_{lk}}{M} + \frac{1}{\mu}\frac{\rho_g}{\rho_c}\frac{m_{ck}}{M} + \frac{1}{P_k}\frac{m_{gk}}{M}\right]. \end{aligned} \tag{9}$$

N_{2l}, N_{2c}, and N_{2g} underline the role of the mass of liquid, crystal and gas, respectively, at a cycle onset. They describe both the influence of the elastic deformation of the surroundings (terms proportional to $1/\mu$) and the compressibility of the different phases. Crystals are assumed to be incompressible, the melt compressibility is equal to $1/\beta_{\text{liq}}$ and the gas compressibility is approximated by $1/P_k$ as the temperature decrease is low during a cycle.

[13] During a given cycle k, the evolution of magma pressure with time is linearized:

$$P \approx P_k + \left[\frac{dP}{dt}\right]_{t_k}(t - t_k). \tag{10}$$

Combining equations (6) and (7), we can write

$$\frac{dP}{dt}(t) = \frac{\frac{1}{M}\frac{d\Delta m_c}{dt} - \left[\frac{\partial f_k(P,T)}{\partial T}\right]_P \frac{dT}{dt}}{\left[\frac{\partial f_k(P,T)}{\partial P}\right]_T}. \tag{11}$$

Given the crystallization law (equation (2)), the magma pressurization rate becomes

$$\frac{dP}{dt}(t) = -\frac{dT}{dt}\frac{\left(\frac{1}{T_l - T_s} + \left[\frac{\partial f_k(P,T)}{\partial T}\right]_P\right)}{\left[\frac{\partial f_k(P,T)}{\partial P}\right]_T}. \tag{12}$$

2.3. Episodic Gas Expulsion

[14] Wall rock failure occurs when magma overpressure exceeds a critical value, which depends both on the mechanism of fracturing and on the system geometry. We assume that fractures are opened in tensile regime, as commonly observed in experiments of forced fluid injections [*Cornet*, 1992]. In this case, host rock fracturing occurs when magma overpressure is twice the tensile strength of the surrounding rocks, assumed constant with time, because the intrusion is spherical [*Tait et al.*, 1989]. Instantaneously, gas escapes and magma pressure returns to the lithostatic pressure. The magma decompression leads to an additional exsolution of a small amount of gas represented by the mass of exsolved gas at the onset of a cycle. This process results in a feedback on magma pressurization (Figure 2, step 3). In section 2.3.1, the expression of the amount of exsolved gas induced by decompression is determined. In section 2.3.2, the simplified formulations of the state equation (equations (6) and (7)) and of the pressurization rate for andesitic magmas are developed.

2.3.1. Mass Fraction of Exsolved Gas at a Cycle Onset

[15] Magma decompression leads to the exsolution of a fraction of volatiles, which remains trapped in the intrusion. This process controls the term N_{2g} (equation (9)), which describes the influence of the mass fraction of exsolved gas λ_{gk} at the onset of a cycle k. Conservation of the mass of volatile species at the kth fracturing event implies

$$\bar{m}_{dk} = m_{g(k+1)} + m_{d(k+1)}, \tag{13}$$

where, for a given cycle, $\bar{m}$ refers to values just before fracturing (see Tables 1 and 2) because all the exsolved gas escapes from the magma at fracturing. Using the solubility law, equation (13) may be rewritten

$$s(P_k + 2\sigma_t)^n \bar{m}_{lk} = m_{g(k+1)} + sP_k^n m_{l(k+1)}. \tag{14}$$

If the mass of volatiles is neglected, the total mass conservation can be written

$$\frac{\bar{m}_{lk}}{M} = \frac{m_{l(k+1)}}{M} = 1 - \frac{m_{c(k+1)}}{M}. \tag{15}$$

Therefore the mass fraction of exsolved gas at the onset of cycle k is

$$\lambda_{gk} = \left[s(P_k + 2\sigma_t)^n - sP_k^n\right]\left(1 - \frac{m_{ck}}{M}\right). \tag{16}$$

It depends on the amount of residual melt and the initial pressure but, more importantly, on the tensile strength of the surrounding rocks, which determines the maximum overpressure and thus the magnitude of decompression.

2.3.2. Pressurization of Andesitic Magmas

[16] Given the range of assumed magma depths (2–10 km) and tensile strengths of the surrounding rocks (0.01–10 MPa) (see section 2.5), pressure variations are low compared to lithostatic pressure and the different terms of the state equation of magma f_k (equation (7)) may consequently be simplified as follows:

$$N_1 \approx n\frac{m_{lk}}{M}\frac{\Delta P}{P_k}, \tag{17}$$

$$\frac{N_{2l}}{N_1} \approx \frac{1}{n}\frac{1}{sP_k^n}\frac{\rho_g}{\rho_l}\left(\frac{1}{\beta_{\text{liq}}} + \frac{1}{\mu}\right)P_k, \tag{18}$$

$$\frac{N_{2c}}{N_1} \approx \frac{1}{n}\frac{1}{sP_k^n}\frac{\rho_g}{\rho_c}\frac{P_k}{\mu}\frac{m_{ck}}{m_{lk}}, \tag{19}$$

$$\frac{N_{2g}}{N_1} \approx \frac{1}{n}\left[\left(1 + \frac{2\sigma_t}{P_k}\right)^n - 1\right] \approx \frac{2\sigma_t}{P_k}. \tag{20}$$

For the set of fixed physical parameters, listed in Table 4, the ratio N_{2l}/N_1 varies within the range 0.01–0.14. Because

of the high water solubility and the low liquid compressibility, the term N_{2l} is negligible compared to the term N_1. The ratio N_{2c}/N_1 is significant only when the mass of residual melt is low. This is not the case in our study, which describes the first stages of crystallization. The value of N_{2g}/N_1 is not well constrained and varies from 10^{-4} to 10^{-1}. Therefore, the term N_{2g} cannot be neglected, especially for high tensile strengths. Finally, the term related to the crystallization contraction varies between -0.3 and -0.7 and has to be accounted for. Neglecting the contribution from the host rock deformation and from the liquid compressibility, the magma equation of state f_k may therefore be approximated by

$$f_k(P,T) \approx \frac{\left[1-\left(\frac{P_k}{P}\right)^n\right]\left(1-\frac{m_{ck}}{M}\right)+\frac{\lambda_{gk}}{sP^n}\left(\frac{P}{P_k}-1\right)}{1+\frac{1}{sP^n}\frac{P}{AT}\left(\frac{1}{\rho_c}-\frac{1}{\rho_l}\right)}, \quad (21)$$

which gives

$$\left[\frac{\partial f_k}{\partial P}\right]_T (P_k,T_k) = \frac{\frac{n}{P_k}\left(1-\frac{m_{ck}}{M}\right)+\frac{\lambda_{gk}}{sP_k^{n+1}}}{1+\frac{1}{sP_k^n}\frac{P_k}{AT_k}\left(\frac{1}{\rho_c}-\frac{1}{\rho_l}\right)} \quad (22)$$

and

$$\left[\frac{\partial f_k}{\partial T}\right]_P (P_k,T_k) = 0. \quad (23)$$

From the magma cooling law (equation (1)), the pressurization of andesitic magmas, induced by melt crystallization and water exsolution, may thus be described by

$$\frac{dP}{dt}(t_k) = \left[\frac{\frac{3a_{\rm th}}{R^{2-3b_{\rm th}}}\left(\frac{\alpha_{\rm th} g}{\nu_k}\right)^{b_{\rm th}} K_{\rm th}^{1-b_{\rm th}}\left(T_k - T_{\rm contact}\right)^{1+b_{\rm th}}}{(T_l - T_s)+\frac{L}{C_p}}\right] \cdot \left[\frac{\frac{n}{P_k}\left(1-\frac{m_{ck}}{M}\right)+\frac{\lambda_{gk}}{sP_k^{n+1}}}{1+\frac{1}{sP_k^n}\frac{P_k}{AT_k}\left(\frac{1}{\rho_c}-\frac{1}{\rho_l}\right)}\right]^{-1}. \quad (24)$$

2.4. Model Outputs

[17] We choose model outputs that may be compared to geophysical and geochemical data characterizing the surficial manifestations of a degassing magma: the time interval Δt between two consecutive gas pulses, the number N of gas pulses since magma intrusion until a given time, the mass fraction ΔG of expelled gas per cycle relative to the initial available mass of gas, and the total mass fraction G of expelled gas. In practice, Δt is more easily estimated because it does not require a gas survey starting at the time of magma intrusion. These outputs are of particular interest because they are directly observable, contrary to other model variables such as magma viscosity, temperature, crystal content and overpressure. The relevant model variables are listed in Table 3.

[18] Mass conservation for the volatile species during a given cycle k yields the following expression of the mass fraction of exsolved gas at the end of the cycle:

$$\frac{\bar{m}_{gk}}{M} = \lambda_{gk} + x_k\left(1-\frac{m_{ck}}{M}\right) - \bar{x}_k\left(1-\frac{\bar{m}_{ck}}{M}\right). \quad (25)$$

This equation may be rewritten

$$\frac{\bar{m}_{gk}}{M} = \lambda_{gk} + sP_k^n\left(1-\frac{m_{ck}}{M}\right) - s(P_k+2\sigma_t)^n\left(1-\frac{\bar{m}_{ck}}{M}\right). \quad (26)$$

The entire exsolved gas is lost at each fracturing event and the cumulative fraction of expelled gas after N cycles is therefore given by

$$\frac{m_g}{M} \approx \sum_{k=1}^{N}\left[\lambda_{gk} + sP_k^n\left(1-\frac{m_{ck}}{M}\right) - s(P_k+2\sigma_t)^n\left(1-\frac{\bar{m}_{ck}}{M}\right)\right]. \quad (27)$$

It follows that G, the total mass of expelled gas relative to the initial available mass of gas $(m_g)_{Max}$ just after intrusion, is

$$G = \frac{m_g}{(m_g)_{\rm Max}} = \sum\nolimits_{k=1}^{N} \Delta_k G, \quad (28)$$

with $\Delta_k G$ the mass fraction of gas expelled at a given cycle k relative to the initial available mass of gas

$$\Delta_k G \approx \frac{\lambda_{gk} + sP_k^n\left(1-\frac{m_{ck}}{M}\right) - s(P_k+2\sigma_t)^n\left(1-\frac{\bar{m}_{ck}}{M}\right)}{sP_i^n\left(1-\frac{m_{ci}}{M}\right)}. \quad (29)$$

2.5. Realistic Range of the Model Input Values

[19] Model inputs are based on a set of initial conditions appropriate for (1) the host rocks, with the tensile strength of the surrounding rocks σ_t, and (2) the magma intrusion, including: the intrusion radius R and depth z, the temperature contrast ΔT between magma and surroundings, and the magma crystallinity Φ_i. They may be divided into two classes. The first class is composed of R, ΔT and Φ_i, which directly control the magma cooling and crystallization processes (Figure 2, step 1). The second class includes z and σ_t, which are involved in the second and third stages of the model, respectively, describing magma pressurization (Figure 2, step 2) and episodic gas expulsion (Figure 2, step 3). Realistic ranges of these model input values may be determined for andesitic magmas.

[20] The model has been run for a range of plausible intrusion sizes (Table 3). Estimation of Φ_i values may be based on petrological studies of andesitic magmas. Most microlites and nanolites form during rapid magma ascent, partly due to melt cooling but mainly to magma degassing. Phenocrysts are mainly formed within magma chamber during slow cooling processes. Thus, we use the phenocryst contents observed in andesitic magmas to estimate the range of Φ_i values. This represents an upper limit of the intrusion crystallinity because rapid phenocryst overgrowth (a few months or less) may happen during magma ascent [*Blundy and Cashman*, 2005]. Ranges are 25–50 vol % at Mount Pelée (Martinique, Lesser Antilles) [*Villemant and Boudon*, 1999]; 35–45 vol % at Soufrière Hills Volcano (Montserrat, Lesser Antilles) [*Sparks et al.*, 2000]; 38–49 vol % at Mount St. Helens (United States) [*Kuntz et al.*, 1981]; and 23–28 vol % at Mount Unzen (Japan) [*Nakada and Motomura*, 1999]. Φ_i is thus assumed to range between 25 and 50 vol %.

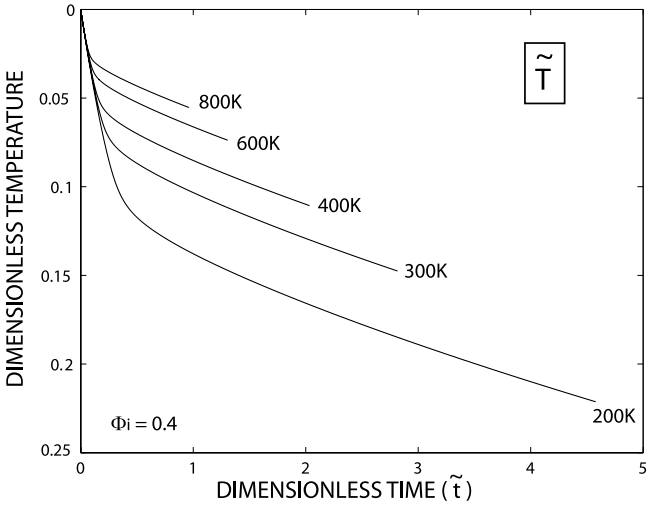


Figure 3. Evolution of dimensionless magma temperature $\tilde{T}$ with dimensionless time $\tilde{t}$, for values of the initial temperature contrast between magma and surrounding rocks ΔT within the range [200–800] K ($\Phi_i = 0.4$). End points of the curves correspond to the time to convection cessation, defined by a magma crystallinity of 60 vol %.

[21] The initial temperature contrast depends on the magma depth and on local thermal anomalies, such as those related to hydrothermal systems, which are generally poorly known. The value of ΔT may vary to a large extent from case to case and a wide range of 200–800 K is assumed.

[22] Constraints given by phase equilibrium and melt inclusion composition indicate that the saturation pressure conditions vary between ~1.1 and 2.2 kbar [*Scaillet and Pichavant*, 2003]. This corresponds to depth between 4.5 and 9 km at lithostatic equilibrium. This range represents upper limits of the magma intrusion depth, which is thus restricted to 2–10 km in the model.

[23] Studies of dike sizes [*Pollard*, 1987] and propagation [*Einarsson and Brandsdottir*, 1980; *Rubin and Pollard*, 1987] may be used to constrain magma overpressures within the range 1–10 MPa. On the basis of laboratory experiments, host rock tensile strengths of ~10 MPa are estimated for granites and basalts [*Touloukian et al.*, 1981]. Such ranges of σ_t values may be considered as upper estimations since, in natural volcanic systems, surrounding rock material may be weakened by fissures and faults. Consequently, we allow for a very wide interval of possible values for σ_t: from 0.01 to 10 MPa. The chosen ranges of values for each model input are summarized in Table 3.

3. Influence of the Initial Conditions on Magma Degassing

[24] Here, we introduce the evolution of magma temperature, viscosity, crystal content and of the model outputs describing magma degassing (Table 3). Different regimes of magma cooling and gas expulsion are distinguished, depending on the initial conditions. In our treatment, we vary the value of one of the model inputs, while holding the others at their midrange or reference value (Table 3). We note that the initial conditions associated to the magma intrusion are unknown in our study and may be considered as parameters. Computations are carried out for a set of fixed physical parameters (Table 4). This discussion will allow us to determine the initial conditions that play a key role in the degassing process.

3.1. Regimes of Magma Cooling

3.1.1. Time Rescaling of the Magma Cooling Process

[25] The magma cooling law (equation (4)) is an equation with separate variables $\tilde{T}$ and $\tilde{t}$. Integration shows that the dimensionless temperature depends only on ΔT and Φ_i:

$$\tilde{T} = \tilde{T}_{\Delta T, \Phi_i}(\tilde{t}). \tag{30}$$

In this notation, variables are in brackets and parameters shown as indices. We note that R has no influence on the evolution of $\tilde{T}$ with $\tilde{t}$. This evolution is shown in Figures 3 and 4 with ΔT and Φ_i, respectively, chosen in their range of

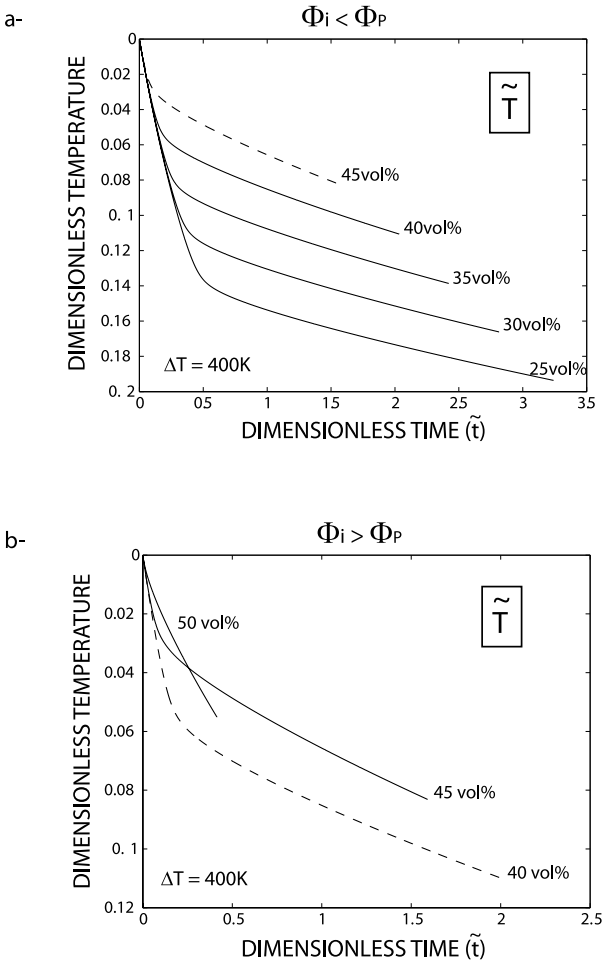


Figure 4. Evolution of dimensionless magma temperature $\tilde{T}$ with dimensionless time $\tilde{t}$, for values of the initial crystal content Φ_i (a) lower than the percolation threshold Φ_P, within the range 25–40 vol %, with the limit case Φ_i = 45 vol % for comparison, and (b) greater than Φ_P, within the range 45–50 vol %, with the limit case Φ_i = 40 vol % for comparison. ΔT is fixed at its reference value of 400 K. End points of the curves correspond to the time to convection cessation, defined by a magma crystallinity of 60 vol %.

Table 5. Range of the Values of the Time t_{conv} to Convection Cessation as a Function of (R, ΔT, Φ_i), According to Equation (34)[a]

Cooling Model Inputs	Realistic Range of Values	Range of t_{conv} (years)	Ratio $\max(t_{conv})/\min(t_{conv})$
R	[5–500] m	[1–457]	3×10^2
ΔT	[200–800] K	[377–56]	~7
Φ_i	[30–50] vol %	[176–145]	~1

[a]Calculations are carried out by varying the value of one of the model input in the realistic range discussed in section 2.5, while holding the others at their midrange or reference value (Table 3), with $C = 1360$, $\alpha_1 = 1.1$, and $\alpha_2 = 1$. The ratio of the maximum value of t_{conv} to its minimum value underlines the influence of each model input.

values (Table 3). For any value of ΔT and for a reference value of Φ_i chosen at midrange, the magma temperature follows a similar evolution, characterized by two cooling rates (Figure 3). Consequently, the cooling process may be rescaled by the time to cessation of convection $\tilde{t}_{conv}$, which can be written

$$\tilde{t}_{conv}(\Delta T, \Phi_i) = \frac{h(\Phi_i)}{\Delta T^{\alpha_1}}, \tag{31}$$

where h is a function depending on Φ_i and α_1 a constant. A least squares fit of the computed values of $\tilde{t}_{conv}$ with ΔT within the range [200–800] K gives $\alpha_1 \approx 1.1$ (correlation coefficient of 0.99).

[26] The evolution of magma temperature, for a set of values of the initial crystal content and a reference value of ΔT, is more complex because different cooling trends are observed depending on Φ_i values. For Φ_i values within the range 25–40 vol %, magma cooling is characterized by two different cooling rates (Figure 4a) as mentioned before. For Φ_i values greater than the crystal percolation threshold Φ_P, no such transition is observed. In the extreme case Φ_i = 50 vol %, viscosity is almost constant and the temperature decrease is monotonous with time (Figure 4b). In what follows, we focus on the case where two regimes of magma cooling are observed. Similarly to the relation determined previously as a function of ΔT variations, the time until convection ceases follows a specific law depending on Φ_i and ΔT. Given equation (31), we can write

$$\tilde{t}_{conv}(\Phi_i, \Delta T) = \frac{C}{\Delta T^{\alpha_1} \Phi_i^{\alpha_2}}, \tag{32}$$

where C and α_2 are two constants. A least squares fit of the computed values of $\tilde{t}_{conv}$ with Φ_i values in the range 25–40 vol % gives $C \approx 1360$ and $\alpha_2 \approx 1$ (correlation coefficient of 0.99). For $\Phi_i \leq \Phi_P$, the evolution of temperature can be expressed as a function of $\breve{t}$:

$$\breve{t} = \frac{\tilde{t}}{\tilde{t}_{conv}} = \frac{t}{t_{conv}}, \tag{33}$$

where t_{conv} is the time to cessation of convection, which is dependent on R, ΔT and Φ_i according to the expression

$$t_{conv}(R, \Delta T, \Phi_i) = C \frac{\tau(R, \Delta T, \Phi_i)}{\Delta T^{\alpha_1} \Phi_i^{\alpha_2}}. \tag{34}$$

In Table 5, we report the estimated range of the values of t_{conv} as a function of (R, ΔT, Φ_i) when these model inputs are set to values within the range discussed in section 2.5. From these calculations, we find that t_{conv} mainly depends on the magma intrusion radius:

$$t_{conv} \approx t_{conv}(R). \tag{35}$$

This implies the same property for the rescaled time:

$$\breve{t} \approx \breve{t}_R(t). \tag{36}$$

Magma temperature consequently becomes

$$\tilde{T} = \tilde{T}_{\Delta T, \Phi_i}(\breve{t}_R). \tag{37}$$

3.1.2. Magma Cooling Transition due to Crystal Percolation

[27] Both the magma viscosity increase and the decrease of the temperature contrast between magma and surroundings lead to a slowing of the magma cooling and crystallization processes. For any values of the initial conditions (ΔT, Φ_i), the temperature decrease with the rescaled time $\breve{t}$ is characterized by two different cooling rates (Figure 5a). During the first cycles after magma intrusion, the cooling rate is large and constant then it changes rapidly to a constant rate about twenty times lower. We find that the transition between these two regimes corresponds to the strong viscosity increase due to the crystal percolation (Figures 5a, 5b, and 5c). Magma viscosity is consequently the key variable controlling temperature. This transition occurs at a critical rescaled cooling time $\breve{t}_C$, which is relatively independent of ΔT and Φ_i. According to equations (33) and (35), the critical time t_C is given to a first approximation by

$$t_C \approx \breve{t}_C t_{conv}(R). \tag{38}$$

and is thus mainly dependent on the value of R, the values of ΔT and Φ_i having only second-order effects. We can consequently write

$$t_C \approx t_C(R), \tag{39}$$

where t_C is an increasing function of R: the larger the magma intrusion, the more delayed the transition of the cooling regime.

[28] As observed in Figure 5c, the evolution of the crystal content with the rescaled time $\breve{t}$, weakly depends on ΔT:

$$\frac{m_c}{M} \approx \left[\frac{m_c}{M}\right]_{\Phi_i}(\breve{t}_R). \tag{40}$$

Magma viscosity (Figure 5b) is directly dependent on the crystal content and is controlled by the same model inputs:

$$\eta \approx \eta_{\Phi_i}(\breve{t}_R). \tag{41}$$

3.2. Regimes of Episodic Gas Expulsion

[29] The influence of each model input (ΔT, Φ_i, z, σ_t) on magma degassing is now analyzed. The evolution of the model outputs (Δt, N, G, ΔG) with the rescaled time $\breve{t}$ is evaluated as a function of the different inputs and summarized in Figure 6. Thus, we determine the initial conditions that play a key role in the degassing process.

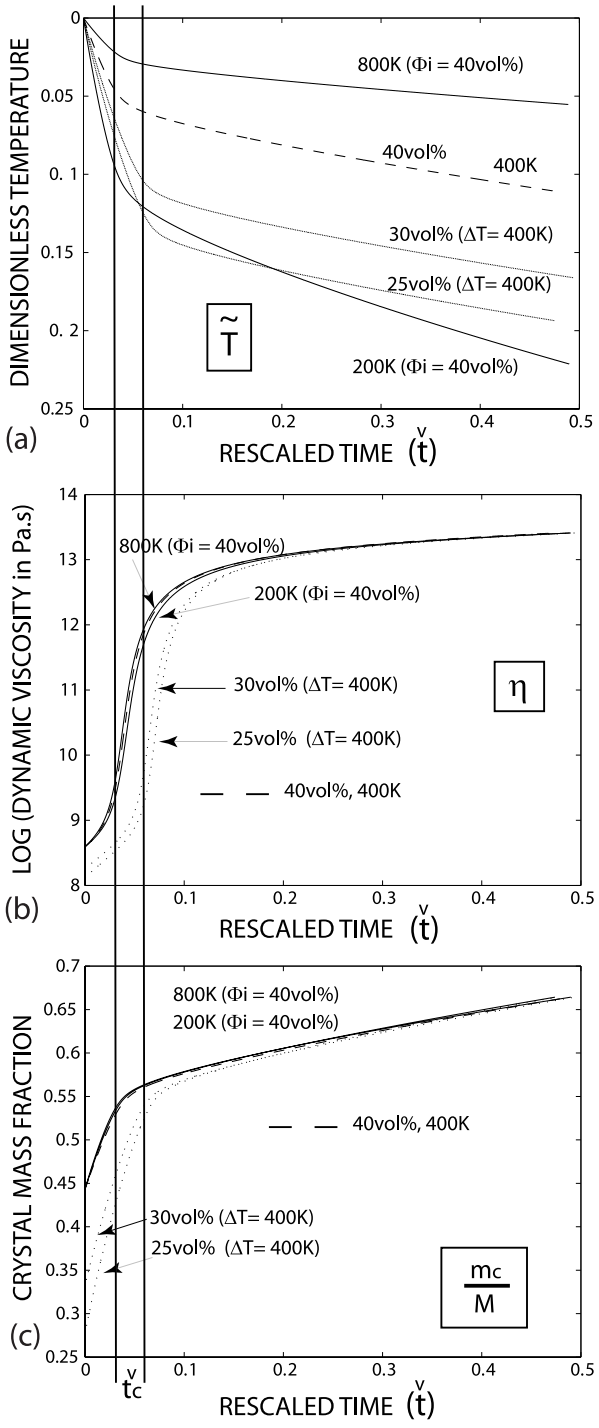


Figure 5. Evolution of (a) dimensionless magma temperature $\tilde{T}$, (b) magma dynamic viscosity η, and (c) crystal mass content with rescaled time $\breve{t}$ for extreme values of ΔT (Φ_i fixed at its reference value of 40 vol %) (line) and Φ_i (ΔT fixed at its reference value of 400 K) (dots), respectively, in their realistic range of values. The dashed line corresponds to the variable evolution for the reference values of the model inputs. The zone delimited by two vertical lines indicates the range of the time $\breve{t}_C$ to the transition in the cooling process.

3.2.1. Number of Gas Pulses and Time Interval Between Two Consecutive Pulses

[30] The degassing process is episodic and the evolution of the number N of gas pulses is a step function. For any values of the model inputs (ΔT, Φ_i, z, σ_t), this evolution follows a similar trend when plotted as a function of the rescaled time $\breve{t}$ (Figure 7). The gas pulse frequency, which is the slope of the curve of N with respect to $\breve{t}$, is large for the first cycles then rapidly drops defining two distinct regimes. These two modes are, of course, also present in the evolution of the time interval Δt between two consecutive pulses (Figure 8). N and Δt present the same dependence relationships with the model inputs. In what follows, these relations are discussed using the evolution of the pulse number. However, the transition between the degassing regimes is described with the evolution of Δt, because it is more clearly visible. It occurs at a critical time $\breve{t}_D$ (D for degassing) associated with the sharp increase in the evolution of Δt. $\breve{t}_D$ is primarily dependent on Φ_i and varies within the range 0.01–0.05 according to Figure 9. It is very close to the transition time of the cooling process $\breve{t}_C$. The decrease of the cooling and crystallization rates with time slows down the gas exsolution and the magma pressurization. The time needed to reach the critical pressure for failure increases, and the gas pulse frequency decreases with time because gas exsolution induced by crystallization is the main process controlling the magma pressurization rate. The timescale and trend of the magma degassing is thus governed by this process.

[31] According to equations (33) and (35), the time to the transition in the degassing process t_D is given by, to a first approximation,

$$t_D \approx \breve{t}_D t_{\mathrm{conv}}(R). \tag{42}$$

The variations of $\breve{t}_D$ with Φ_i are negligible compared to the variations of t_{conv} with R. Consequently, t_D mainly depends on R:

$$t_D \approx t_D(R), \tag{43}$$

	N	Δt	G	ΔG
ΔT	→	→	→	→
Φi	↘ (x 2/3)	↗ (x 3/2)	↘ (x 2/3)	↗ (x 3/2)
z	↗ (x 7)	↘ (x 1/7)	→	→
σ	↘ (x 1/1000)	↗ (x 1000)	→	↗ (x 1000)

Figure 6. Evolution of the model outputs as a function of the different inputs (ΔT, Φ_i, z, σ_t), for a particular rescaled time $\breve{t}$. Arrows specify the sense of variation while the information in brackets indicates the amplitude of variation at the time of convection cessation.

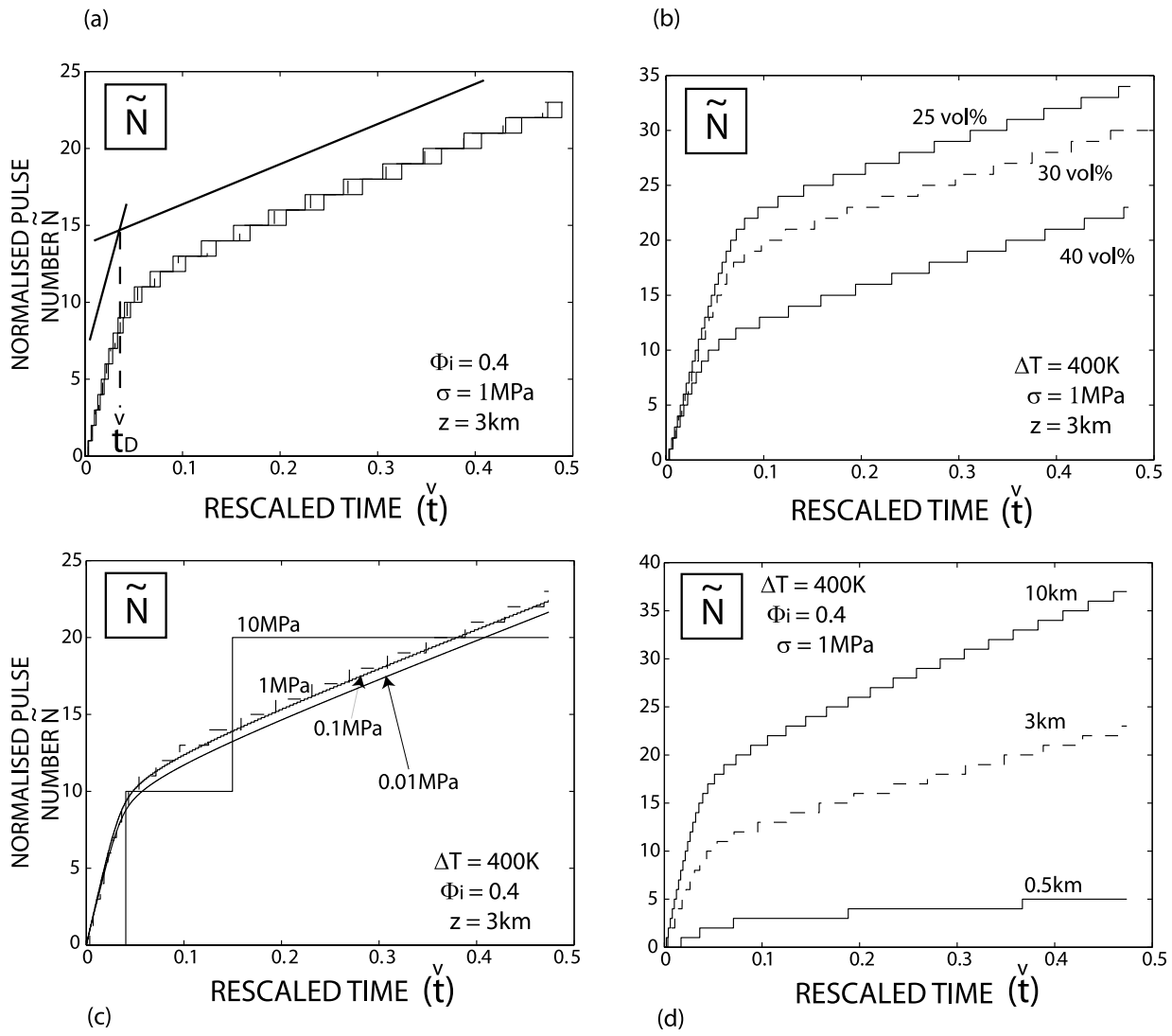


Figure 7. Evolution of the normalized number $\tilde{N}$ of gas pulses (equation (44) with $\sigma_{t(ref)}$ taken equal to 1 MPa) plotted as a function of the rescaled time $\breve{t}$, for different values of (a) ΔT, the initial temperature contrast between magma and surrounding rocks in [200–800] K (black lines underline the transition between the different degassing regimes), (b) Φ_i, the initial magma crystallinity, (c) σ_t, the tensile strength of the host rocks, and (d) z, the magma depth, in their realistic range of values (Table 3). The other model inputs are fixed at their midrange or reference value (Table 3).

where t_D is an increasing function of R: the larger the magma intrusion, the more delayed the transition between the degassing regimes.

[32] Now we discuss the magnitude of the degassing process in terms of the number of gas pulses, according to each model input (Figure 7). It is mainly the tensile strength of the surrounding rocks that controls the magnitude of the degassing (Figure 7c). This model input particularly constrains the critical overpressure needed for wall rock failure (see section 2.3). Given the proportionality of the critical overpressure with σ_t and because, to a first approximation, magma overpressure increases linearly with time during a cycle, a normalized pulse number $\tilde{N}$ may be introduced with

$$N = \tilde{N}\frac{\sigma_{t(ref)}}{\sigma_t}, \tag{44}$$

with $\sigma_{t(ref)}$ a reference value of the host rock tensile strength which is arbitrarily chosen. Similarly,

$$\Delta t = \Delta\tilde{t}\frac{\sigma_t}{\sigma_{t(ref)}}. \tag{45}$$

At a given time, the greater σ_t, the larger the critical overpressure and the smaller the pulse number. The influence of the critical overpressure on N is significant because it varies over several orders of magnitude, according to the range of values of σ_t. Consequently, fracturing is the major process controlling the magnitude of magma degassing.

[33] For a given scaled time $\breve{t}$, the pulse number increases with the depth of magma storage z (Figure 7d). The magma depth influences the degassing via the gas solubility law, which governs the volatile exsolution. According to this

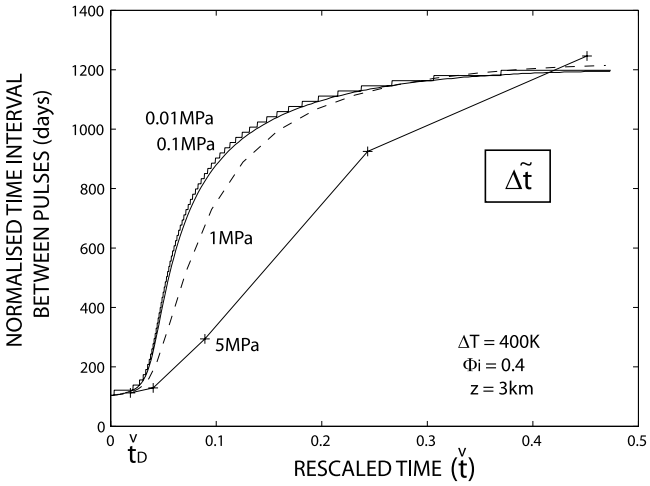


Figure 8. Evolution of the normalized time interval $\Delta\tilde{t}$ between gas pulses (equation (45) with $\sigma_{t(ref)}$ taken equal to 1 MPa) plotted as a function of the rescaled time $\breve{t}$, for different values of the tensile strength of the host rocks σ_t in [0.01–5] MPa. The other model inputs are fixed at their midrange or reference value (Table 3).

law, the deeper the magma intrusion, the larger the quantity of dissolved gas available for exsolution. Consequently, for a given increase of the crystal mass, the magma pressurization and the host rock failure are all the more rapid and the pulse number important that z is large. When convection ceases, the pulse number is proportional to $\sqrt{z}$. This is in agreement with the solubility of water in a rhyolitic melt, which is proportional to the square root of the lithostatic pressure.

[34] At a given time $\breve{t}$, the pulse number increases with decreasing initial crystal content (Figure 7b). A lower Φ_i induces a lower magma viscosity. It follows that the cooling and crystallization rates are consequently higher. Finally, this implies a larger pressurization rate and a higher pulse number at a given time.

[35] Figure 7a shows that variations of the initial temperature contrast ΔT do not significantly modify the evolution of N with $\breve{t}$, as expected from the weak role of this input in the crystallization process.

[36] Figure 7 also shows that the number of gas pulses is quite independent of ΔT and varies, in order of decreasing importance, with σ_t (3 magnitude orders), z and Φ_i. In conclusion, N is mainly dependent on σ_t:

$$N \approx N_{\sigma_t}(\breve{t}_R). \tag{46}$$

Equivalently, Δt is approximated by

$$\Delta t \approx \Delta t_{\sigma_t}(\breve{t}_R). \tag{47}$$

During the first cycles after magma intrusion, the degassing rate is high and approximately constant then it decreases to a new rate ten times lower. According to equation (44) and to the chosen value of σ_t (Table 3), between 2 and 2000 gas pulses may be observed until convection ceases. According to Figure 8, the scaled pulse frequency $\Delta\tilde{t}_1$ is equal to ~100 days in the first regime. In the second, the scaled frequency is about ten times greater $\Delta\tilde{t}_2 \approx 1200$ days (Figure 8). Given equation (45), it follows that Δt_1 ranges between 1 day and 3 years and Δt_2 between 10 days and 30 years, depending on the value of σ_t.

3.2.2. Mass Fraction of Expelled Gas per Pulse

[37] For any value of Φ_i, σ_t, and z, the mass fraction of expelled gas per pulse, relative to the initial available mass of gas just after intrusion, globally decreases with time (Figure 10). To a first approximation, ΔG is proportional to the critical pressure needed for host rock failure. It consequently increases with σ_t and may be normalized by

$$\Delta\tilde{G} = \Delta G \frac{\sigma_{t(ref)}}{\sigma_t}. \tag{48}$$

In a second-order approximation, two patterns are observed according to the value of the tensile strength of the host rocks. For $\sigma_t \leq 0.5$ MPa, $\Delta\tilde{G}$ presents an oscillation occurring close to the critical transition time $\breve{t}_D$ leading to maximum relative variations of 50%. It is all the more significant that σ_t is high. For $\sigma_t < 0.5$ MPa, this effect is negligible and ΔG decreases with time.

[38] Figure 11 shows that the mass of expelled gas varies, in order of decreasing importance, with σ_t, z, and Φ_i, similarly with the number of gas pulses:

$$\Delta G \approx \Delta G_{\sigma_t}(\breve{t}_R). \tag{49}$$

The largest mass of gas expelled per pulse escapes in the first cycles and represents between 0.02 and 20% of the initial mass of gas available in the magma intrusion, depending on the value of σ_t (Table 3).

3.2.3. Total Mass Fraction of Expelled Gas

[39] Figure 12 illustrates the evolution of the total mass fraction G of expelled gas, relative to the initial available mass of

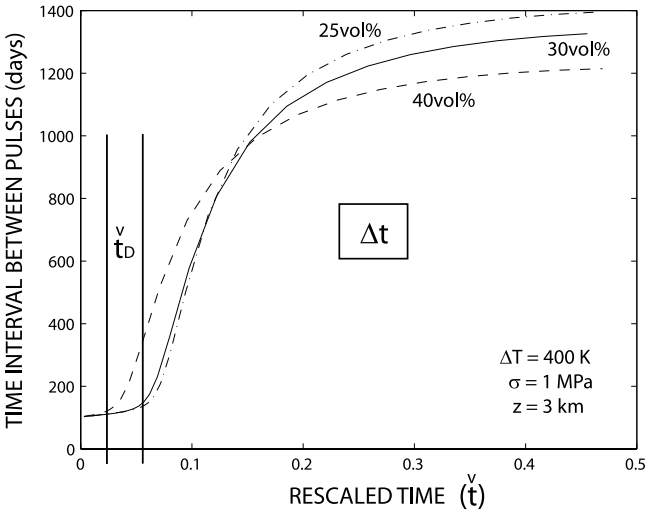


Figure 9. Evolution of the time interval Δt between two consecutive gas pulses, in days, plotted as a function of the rescaled time $\breve{t}$, for different values of the initial crystal content Φ_i in [25–40] vol %. The zone delimited by two vertical lines indicates the range of the time $\breve{t}_D$ to transition in the degassing process. It is defined as the start time of the sharp increase of Δt with time. The other model inputs are fixed at their midrange or reference value (Table 3).

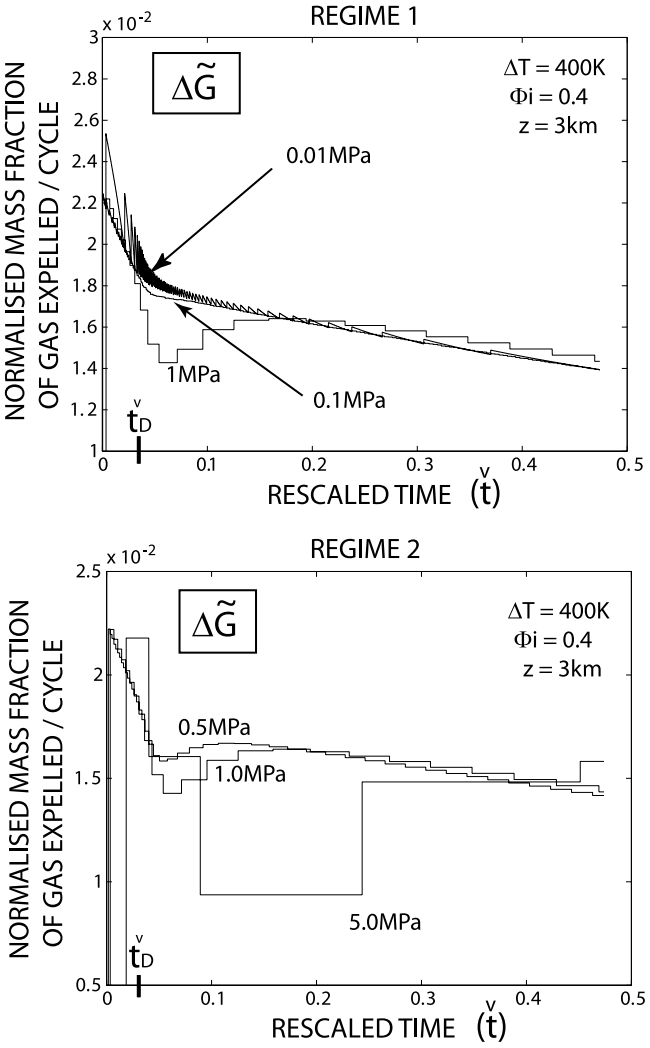


Figure 10. Different regimes observed in the evolution of the normalized mass fraction of expelled gas per pulse $\Delta\tilde{G}$ (equation (48) with $\sigma_{t(ref)}$ taken equal to 1 MPa) plotted as a function of the rescaled time $\breve{t}$, according to the value of the tensile strength of the host rocks σ_t in its realistic range. The other model inputs are fixed at their midrange or reference value (Table 3). The time $\breve{t}_D$ to the transition in the degassing process is specified.

gas just after intrusion. It has the same characteristic trend as the pulse number N, with a changing slope close to the transition time of the degassing process $\breve{t}_D$. However, it is independent of the tensile strength of the surrounding rocks and magma depth. Indeed G depends both on the number of gas pulses and the mass of gas expelled per cycle. Because ΔG varies little with time and thus may be assumed constant, G is approximated by $G \approx N\Delta G$ and presents the same trend as N with time. According to equations (44) and (48), G is consequently independent of σ_t, to a first approximation. The greater the tensile strength the longer the cycle duration, but also the larger the mass of gas expelled per pulse.

[40] For a given time, if we neglect the mass fraction of exsolved gas λ_g at cycle onset, both the initial available mass of gas $(m_g)_{Max}$ and the mass m_g of expelled gas depend on the square root of z according to the solubility law of water in the melt. Their ratio G is thus independent of magma depth.

[41] Therefore, to a first approximation, the total mass fraction of expelled gas mainly depends on the initial crystal content:

$$G \approx G_{\Phi_i}(\breve{t}_R). \tag{50}$$

At the transition time, between 20 and 30% of the initial available mass of gas is expelled. The first pulses imply a high gas loss rate which drops to a constant rate approximately twenty times lower after this transition.

4. Conclusions

[42] For andesitic volcanoes, we interpret episodic patterns of magma degassing, spanning a few years to decades, as the result of the cooling, crystallization and

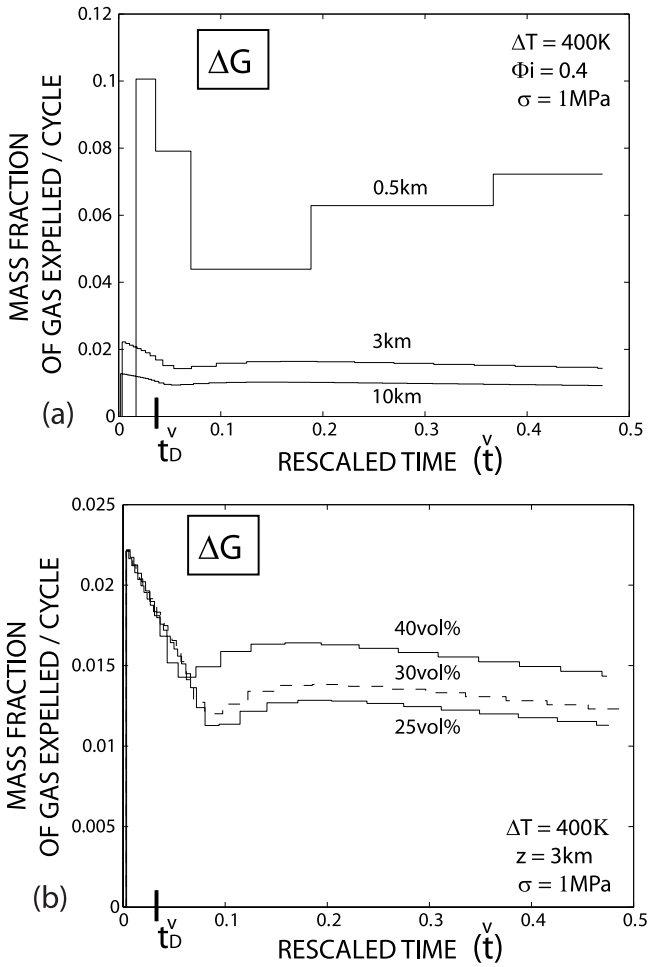


Figure 11. Evolution of the mass fraction of expelled gas per pulse ΔG plotted as a function of the rescaled time $\breve{t}$, for different values of (a) magma depth z in its realistic range of values and (b) initial magma crystallinity Φ_i in [25–40] vol %. The other model inputs are fixed at their midrange or reference value (Table 3). The time $\breve{t}_D$ to the transition in the degassing process is specified.

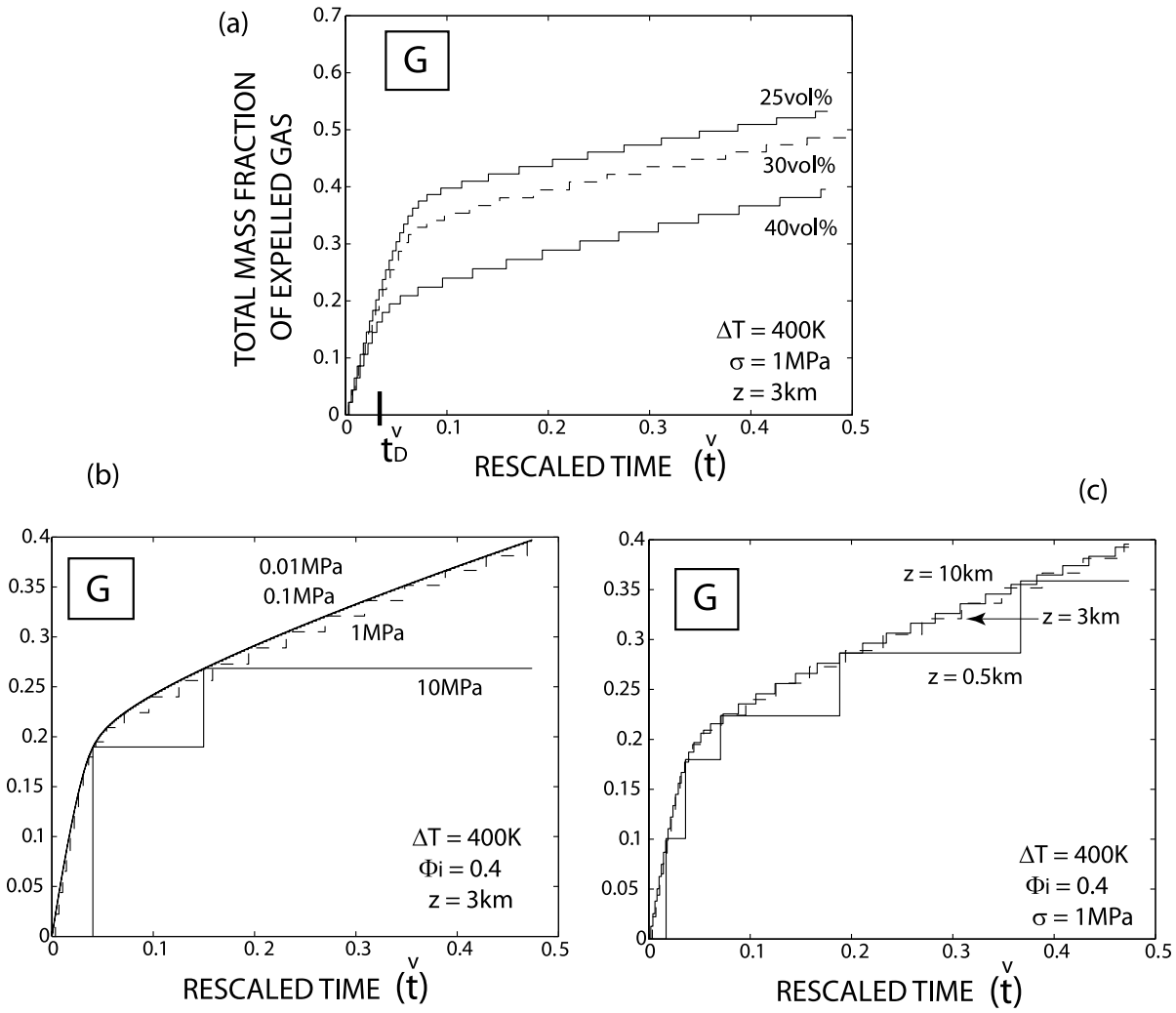


Figure 12. Evolution of the total mass fraction G of expelled gas plotted as a function of the rescaled time $\breve{t}$, for different values of (a) initial magma crystallinity Φ_i, (b) tensile strength of the host rocks σ_t, and (c) magma depth z, in their realistic range of values (Table 3). The other model inputs are fixed at their midrange or reference value (Table 3). The transition time of the degassing process $\breve{t}_D$ is specified.

degassing of a magma intrusion at shallow depth. When the magma crystallinity exceeds the crystal percolation threshold, magma viscosity significantly increases. This process strongly controls the time evolution of all the variables involved in the model (Figure 13). Two regimes of cooling are predicted with time, characterized by different cooling rates. They imply two modes of degassing defined by a high frequency of gas pulses at the beginning of the process and then by a frequency about ten times lower. This change in the degassing regime is the main characteristic of the proposed model.

[43] The trend and timescale of the degassing process are controlled by the gas exsolution induced by melt crystallization. The transition between the degassing regimes occurs at a specific time dependent on the stored magma volume to a first approximation. Between 20 and 30% of the initial available mass of gas has already been expelled by this time. At a given time, the number of gas pulses, the time interval between two consecutive pulses, and the mass fraction of gas expelled per pulse are governed by the mechanism of host rock fracturing, which depends on the wall rock tensile strength.

[44] The comparison between model outputs and gas data allows estimation of the key parameters associated with the degassing magmatic system. Even though the gas transfer from the magma intrusion up to the surface may be modified by a hydrothermal system, we expect that the tensile strength of the surrounding rocks may be deter-

Figure 13. Evolution with rescaled time $\breve{t}$ for the model inputs at their reference values ($\Delta T = 400$ K, $\Phi_i = 0.4$, $\sigma_t = 1$ MPa and $z = 3$ km) of (left) the relevant model variables (magma dynamic viscosity η, crystal mass fraction m_c/M, dimensionless temperature $\tilde{T}$ and overpressure ΔP); (right) the normalized model outputs describing gas expulsion ($\Delta\tilde{t}$, $\tilde{N}$, G, $\Delta\tilde{G}$). Variables with a tilde refer to the normalized values of the variables according to equations (45), (44), and (48) with $\sigma_{t(ref)}$ taken equal to 1 MPa. The time $\breve{t}_D$ to the transition in the degassing process is mentioned.

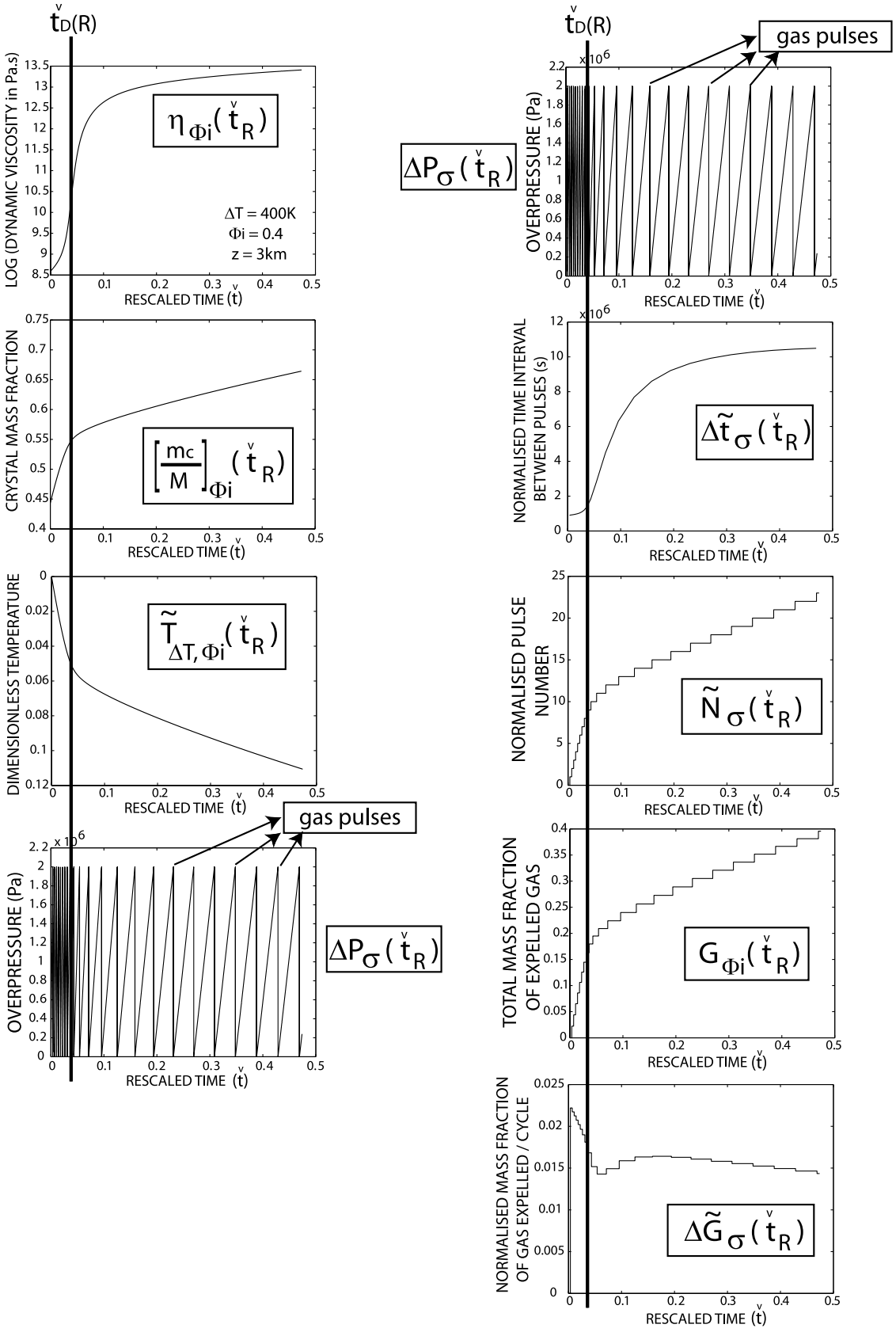

$\hat{t}_D(R)$
LOG (DYNAMIC VISCOSITY in Pa.s)
$\eta_{\Phi i}(\hat{t}_R)$
ΔT = 400K
Φi = 0.4
z = 3km
RESCALED TIME $(\hat{t})$
CRYSTAL MASS FRACTION
$\left[\frac{mc}{M}\right]_{\Phi i}(\hat{t}_R)$
DIMENSIONLESS TEMPERATURE
$\tilde{T}_{\Delta T,\Phi i}(\hat{t}_R)$
gas pulses
OVERPRESSURE (Pa)
$\Delta P_\sigma(\hat{t}_R)$
NORMALISED TIME INTERVAL BETWEEN PULSES (s)
$\Delta\tilde{t}_\sigma(\hat{t}_R)$
NORMALISED PULSE NUMBER
$\tilde{N}_\sigma(\hat{t}_R)$
TOTAL MASS FRACTION OF EXPELLED GAS
$G_{\Phi i}(\hat{t}_R)$
NORMALISED MASS FRACTION OF GAS EXPELLED / CYCLE
$\Delta\tilde{G}_\sigma(\hat{t}_R)$

Figure 13

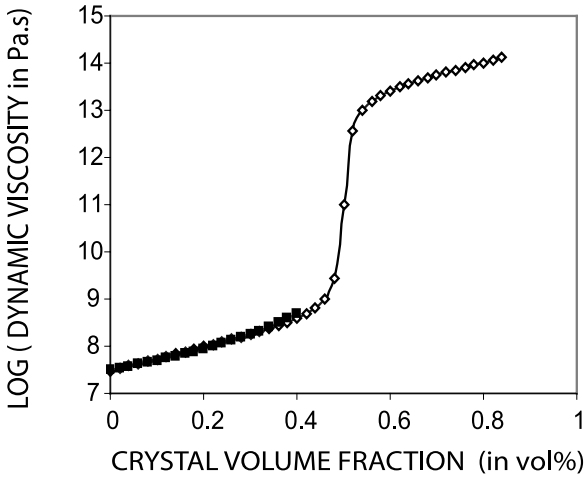


Figure A1. Proposed analytical viscosity law (open diamonds) as a function of the crystal volume fraction, defined by equation (A1) with the set of parameters (Φ_{inflex} = 0.5, log η_{inflex} = 11, A_{incl} = 2.4, B_{asympt} = 1.5, C_{slope} = 80). It verifies the Roscoe law (squares) characterized by (n_R = 2.5, Φ_m = 60 vol %) for crystal fractions smaller than the crystal percolation threshold Φ_P assumed equal to 40 vol %, and is in agreement with experimental results from *Lejeune and Richet* [1995].

mined by geochemical survey with suitable sampling frequency. After magma intrusion, the time interval between pulses predicted by the model ranges between 1 d and 3 years, depending on the value of σ_t within the range 0.01–10 MPa. The mass of expelled gas per pulse is almost constant with time, within the range 0.01–10% of the initial available mass of gas. Using a sustained monitoring record, the identification of a transition in the magma degassing regime would provide an estimate of the stored magma volume. Assuming a realistic range of R values to be 5–500 m, i.e., corresponding to a magma volume of 0.5×10^{-6} to 0.5 km^3, this transition is predicted to occur within the range 3 weeks to 16 years after the magma emplacement.

[45] The estimation of the size of a magma intrusion is of particular relevance for monitoring purposes. An intrusion may perturb the volcanic system over a long duration by degassing. Moreover it may considerably weaken the volcanic edifice and favor flank collapses, as often observed in andesitic volcanoes. A future paper (M. Boichu et al., Degassing at La Soufrière de Guadeloupe volcano (Lesser Antilles) since the last eruptive crisis in 1975–1977: Result of a shallow magma intrusion?, unpublished manuscript, 2007) applies the model to interpret the long-term geochemical data collected at La Soufrière de Guadeloupe volcano (Lesser Antilles), which exhibits two distinct regimes of magma degassing, illustrating the potential relevance of this model for volcanic hazard assessment.

Appendix A: Analytical Dependence Law of Viscosity on Crystal Fraction

[46] We propose an analytical law for the dependence of magma viscosity on crystal volume fraction, which reproduces the trend showed by the experimental results of *Lejeune and Richet* [1995]:

$$\log \eta = \log \eta_{\text{inflex}} + A_{\text{incl}}(\Phi - \Phi_{\text{inflex}}) + B_{\text{asympt}} Arctan\left[C_{\text{slope}}(\Phi - \Phi_{\text{inflex}})\right]. \quad \text{(A1)}$$

This relation depends on five nonindependent parameters. Φ_{inflex} and η_{inflex} represent the crystal volume fraction and the magma viscosity at the inflexion point of the viscosity curve, A_{incl} defines the inclination of its parallel asymptotes, B_{asympt} is the distance between them, and C_{slope} is the curve slope at the inflexion point.

[47] The coefficient A_{incl} is constrained by the Roscoe law $\eta = \eta_0(1 - \Phi/\Phi_m)^{-n_R}$ [*Roscoe*, 1952], which describes the linear variations of viscosity for a crystal fraction smaller than the percolation threshold; n_R is an adjustable parameter and Φ_m the crystal volume fraction preventing any liquid movement. Most experimental measurements are well fitted for n_R = 2.5 and Φ_m = 0.6 [*Marsh*, 1981; *Lejeune and Richet*, 1995]. Viscosity of homogeneous rhyolitic liquids lies within the range 10^7–10^9 Pa s at 1200 K, according to theoretical and experimental studies [*Hess and Dingwell*, 1996; *Neuville et al.*, 1993]. For a crystal fraction $\geq \Phi_m$, magma behaves as a solid and viscosity reaches a relatively constant level around 10^{13}–10^{14} Pa s, regardless of the type of material [*Lejeune and Richet*, 1995]. This controls the value of B_{asympt}. Given η_0, A_{incl} and B_{asympt}, the value of η_{inflex} is constrained. Finally, Φ_{inflex} and C_{slope} are both linked to the percolation threshold associated to a crystal fraction of ~40 vol %. Figure A1 illustrates the viscosity law that we propose for andesitic magmas.

[48] **Acknowledgments.** We are particularly grateful to Claude Jaupart for many discussions about the model and to Clive Oppenheimer for his careful reading which helped to improve the manuscript. The manuscript benefited from the constructive and critical comments of David Pyle and an anonymous reviewer. This manuscript is the IPGP contribution 2340.

References

Allard, P. (1997), Endogeneous degassing and storage at Mount Etna, *Geophys. Res. Lett.*, *24*, 2219–2222.

Bagdassarov, N., D. Dingwell, and M. Wilding (1996), Rhyolite magma degassing: An experimental study of melt vesiculation, *Bull. Volcanol.*, *57*, 587–601.

Bejan, A. (1984), *Convection Heat Transfer*, John Wiley, New York.

Blake, S. (1984), Volatile oversaturation during the evolution of silicic magma chambers as an eruption trigger, *J. Geophys. Res.*, *89*(B10), 8237–8244.

Blundy, J., and K. Cashman (2005), Rapid decompression-driven crystallisation recorded by melt inclusions from Mount St-Helens volcano, *Geology*, *33*(10), 793–796.

Burnham, C. (1962), A method for determining the solubility of water in silicate melts, *Am. J. Sci.*, *260*, 721–745.

Burnham, C. (1975), Water and magmas: A mixing model, *Geochim. Cosmochim. Acta*, *39*, 1077–1084.

Carslaw, H., and J. Jaeger (1986), *Conduction of Heat in Solids*, 2nd ed., Clarendon, Oxford, U.K.

Chiodini, G., M. Todesco, S. Caliro, C. Del Gaudio, G. Macedonio, and M. Russo (2003), Magma degassing as a trigger of bradyseismic events: The case of Phlegrean Fields (Italy), *Geophys. Res. Lett.*, *30*(8), 1434, doi:10.1029/2002GL016790.

Churchill, S., and R. Usagi (1972), A general expression for the correlation of rates of transfer and other phenomena, *AIChE J.*, *18*, 1121–1128.

Cornet, F. (1992), Fracture processes induced by forced fluid percolation, in *Volcanic Seismology*, edited by P. Gasparini, R. Scarpa, and K. Aki, *IAVCEI Proc. Volcanol.*, 3, 407–431.

Edmonds, M., C. Oppenheimer, D. Pyle, R. Herd, and G. Thompson (2003), SO_2 emissions from Soufrière Hills Volcano and their relationship to conduit permeability, hydrothermal interaction and degassing regime, *J. Volcanol. Geotherm. Res.*, *124*, 23–43.

Einarsson, P., and B. Brandsdottir (1980), Seismological evidence for lateral magma intrusion during the July 1978 deflation of the Krafla volcano in NE Iceland, *J. Geophys.*, *47*, 160–165.

Feuillard, M., C. Allègre, G. Brandeis, R. Gaulon, J. Le Mouel, J. Mercier, J. Pozzi, and M. Semet (1983), The 1975–1977 crisis of La Soufrière de Guadeloupe: A still-born magmatic eruption, *J. Volcanol. Geotherm. Res.*, *16*, 317–334.

Fischer, T., M. M. Morrissey, M. L. V. Calvache, D. M. Gomez, R. C. Torres, J. Stix, and S. Williams (1994), Correlations between SO_2 flux and long-period seismicity at Galeras Volcano, *Nature*, *368*, 135–137.

Fischer, T., G. Arehart, N. Sturchio, and S. Williams (1996), The relationship between fumarole gas composition and eruptive activity at Galeras Volcano, Colombia, *Geology*, *24*, 531–534.

Francis, P., C. Oppenheimer, and D. Stevenson (1993), Endogenous growth of persistently active volcanoes, *Nature*, *366*, 554–557.

Giggenbach, W., and D. Sheppard (1989), Variations in the temperature and chemistry of White Island fumarole discharges 1972–85, *N. Z. Geol. Surv. Bull.*, *103*, 119–126.

Harris, A., and A. Maciejewski (2000), Thermal surveys of the Vulcano Fossa fumarole field 1994–1999: Evidence for fumarole migration and sealing, *J. Volcanol. Geotherm. Res.*, *102*, 119–147.

Hess, K.-U., and D. Dingwell (1996), Viscosities of hydrous leucogranitic melts: A non Arrhenian-model, *Am. Mineral.*, *81*, 1297–1300.

Ingebritsen, S., D. Galloway, E. Colvard, M. Sorey, and R. Mariner (2001), Time-variation of hydrothermal discharge at selected sites in the western United States: Implications for monitoring, *J. Volcanol. Geotherm. Res.*, *111*, 1–23, doi:10.1016/S0377-0273(01)00207-4.

Kazahaya, K., H. Shinohara, and G. Saito (2002), Degassing process of Satsuma-Iwojima volcano, Japan: Supply of volatile components from a deep magma chamber, *Earth Planets Space*, *54*, 327–335.

Komorowski, J.-C., G. Boudon, M. Semet, F. Beauducel, C. Anténor-Habazac, S. Bazin, G. Hammouya, and J.-L. Cheminée (2005), Guadeloupe, in *Volcanic Atlas of the Lesser Antilles*, edited by J. M. Lindsay et al., pp. 63–100, Seismic Res. Unit, Univ. of the West Indies, Saint Augustine, Trinidad and Tobago.

Kuntz, M., P. Rowley, N. MacLeod, R. Reynolds, L. MacBroome, A. Kaplan, and D. Lidke (1981), Petrography and particle-size distribution of pyroclastic-flow, ash-cloud, and surge deposits, *U.S. Geol. Surv. Prof. Pap.*, *1250*, 525–539.

Lejeune, A. (1994), Rhéologie des magmas: Influence des cristaux et des bulles en suspension, Ph.D. thesis, Univ. Paris 7–Denis Diderot, Paris.

Lejeune, A., and P. Richet (1995), Rheology of crystal-bearing silicate melts: An experimental study at high viscosities, *J. Geophys. Res.*, *100*(B3), 4215–4229.

López, D., J. Bundschuh, G. Soto, J. Fernández, and G. Alvarado (2006), Chemical evolution of thermal springs at Arenal Volcano, Costa Rica: Effect of volcanic activity, precipitation, seismic activity, and Earth tides, *J. Volcanol. Geotherm. Res.*, *167*, 166–181.

Marsh, B. (1981), On the crystallinity, probability of occurence, and rheology of lava and magma, *Contrib. Mineral. Petrol.*, *78*, 85–98.

Marsh, B. (2000), Magma chambers, in *Encyclopedia of Volcanoes*, pp. 191–206, Academic, New York.

Martin, D., and R. Nokes (1989), A fluid-dynamical study of crystal settling in convecting magmas, *J. Petrol.*, *30*(6), 1471–1500.

Milliken, W., M. Gottlieb, A. Graham, L. Mondy, and R. Powell (1989), The viscosity-volume fraction relation for suspensions of rod-like particles by falling-ball rheometry, *J. Fluid. Mech.*, *202*, 217–232.

Nakada, S., and Y. Motomura (1999), Petrology of the 1991–1995 eruption at Unzen: Effusion pulsation and groundmass crystallisation., *J. Volcanol. Geotherm. Res.*, *89*, 173–196.

Neuville, D., P. Courtial, D. Dingwell, and P. Richet (1993), Thermodynamic and rheological properties of rhyolite and andesite melts, *Contrib. Mineral. Petrol.*, *113*, 572–581.

Nicholls, J., and M. Stout (1982), Heat effects of assimilation, crystallisation and vesiculation in magmas, *Contrib. Mineral. Petrol.*, *81*, 328–339.

Nuccio, P., and A. Paonita (2001), Magmatic degassing of multicomponent vapors and assessment of magma depth: Application to Vulcano Island (Italy), *Earth Planet. Sci. Lett.*, *193*, 467–481.

Pollard, D. (1987), Elementary fracture mechanics applied to the structural interpretation of dykes, in *Mafic Dyke Swarms*, edited by H. C. Halls and W. F. Fahrig, *Geol. Assoc. Can. Spec. Pap.*, *34*, 5–24.

Richet, P., and Y. Bottinga (1986), Thermochemical properties of silicate glasses and liquids: A review, *Rev. Geophys.*, *24*, 1–25.

Richet, P., A. Lejeune, F. Holtz, and J. Roux (1996), Water and the viscosity of andesite melts, *Chem. Geol.*, *128*, 185–197.

Roscoe, R. (1952), The viscosity of suspensions of rigid spheres, *Br. J. Appl. Phys.*, *3*, 267–269.

Rowe, G., S. Ohsawa, B. Takano, S. Brantley, J. Fernandez, and J. Barquero (1992), Using Crater Lake chemistry to predict volcanic activity at Poas Volcano, Costa Rica, *Bull. Volcanol.*, *54*, 494–503.

Rubin, A. (1995a), Getting granite dikes out of the source region, *J. Geophys. Res.*, *100*, 5911–5929.

Rubin, A. (1995b), Propagation of magma-filled cracks, *Annu. Rev. Earth Planet. Sci.*, *23*, 287–336.

Rubin, A., and D. Pollard (1987), Origins of blade-like dikes in volcanic rift zones, *U.S. Geol. Surv. Prof. Pap.*, *1350*, 1449–1470.

Rutgers, I. (1962), Relative viscosity of suspensions of rigid spheres in Newtonian liquids, *Rheol. Acta*, *2*, 202–210.

Ryerson, F., H. Weed, and A. Piwinskii (1988), Rheology of subliquidus magmas: 1. Picritic compositions, *J. Geophys. Res.*, *93*, 3421–3436.

Scaillet, B., and M. Pichavant (2003), Experimental constraints on volatile abundances in arc magmas and their implications for degassing processes, in *Volcanic Degassing*, edited by C. Oppenheimer, D. M. Pyle, and J. Barclay, *Geol. Soc. Spec. Publ.*, 213, 23–52.

Shaw, H. (1969), Rheology of basalt in the melting range, *J. Petrol.*, *10*, 510–535.

Shinohara, H., K. Kazahaya, G. Saito, N. Matsushima, and Y. Kawanabe (2002), Degassing activity from Iwodake rhyolitic cone, Satsuma-Iwojima volcano, Japan: Formation of a new degassing vent, 1990–1999, *Earth Planets Space*, *54*, 175–185.

Sparks, R., M. Murphy, A. Lejeune, R. Watts, J. Barclay, and S. Young (2000), Control on the emplacement of the andesite lava dome of the Soufriere Hills volcano, Montserrat by degassing-induced crystallisation, *Terra Nova*, *12*, 14–20.

Spera, F. (1980), Thermal evolution of plutons: A parameterized approach, *Science*, *207*, 299–301.

Spera, F. (2000), Physical properties of magmas, in *Encyclopedia of Volcanoes*, pp. 171–189, Academic, New York.

Stevenson, D., and S. Blake (1998), Modelling the dynamics and thermodynamics of volcanic degassing, *Bull. Volcanol.*, *60*, 307–317.

Stevenson, R., N. Bagdassarov, D. Dingwell, and C. Romano (1998), The influence of trace amounts of water on the viscosity of rhyolites, *Bull. Volcanol.*, *60*, 89–97.

Symonds, R. B., T. M. Gerlach, and M. H. Reed (2001), Magmatic gas scrubbing: Implications for volcano monitoring, *J. Volcanol. Geotherm. Res.*, *108*, 303–341.

Tait, S., C. Jaupart, and S. Vergniolle (1989), Pressure, gas content and eruption periodicity of a shallow, crystallising magma chamber, *Earth Planet. Sci. Lett.*, *92*, 107–123.

Touloukian, Y., J. W. Rudd, and R. Roy (1981), *Physical Properties of Rocks and Minerals, Data Ser. Mater. Prop.*, vols. 1–2, McGraw-Hill, New York.

Villemant, B., and G. Boudon (1999), H_2O and halogen (F,Cl, Br) behaviour during shallow magma degassing processes, *Earth Planet. Sci. Lett.*, *168*, 271–286.

Villemant, B., G. Hammouya, A. Michel, M. P. Semet, J.-C. Komorowski, G. Boudon, and J.-L. Cheminée (2005), The memory of volcanic waters: Shallow depth magma degassing revealed by halogen monitoring in thermal springs of La Soufrière volcano (Guadeloupe, Lesser Antilles), *Earth Planet. Sci. Lett.*, *237*, 710–728.

Ward, S., and R. Whitmore (1950a), Studies of the viscosity and sedimentation of suspensions, part 1–The viscosity of suspension of spherical particles, *Br. J. Appl. Phys.*, *1*, 286–290.

Ward, S., and R. Whitmore (1950b), Studies of the viscosity and sedimentation of suspensions, part 2–The viscosity and sedimentation of suspension of rough powders, *Br. J. Appl. Phys.*, *2*, 325–328.

White, N., and R. Herrington (2000), Mineral deposits associated with volcanism, in *Encyclopedia of Volcanoes*, pp. 897–912, Academic, New York.

Wildemuth, C., and M. Williams (1985), A new interpretation of viscosity and yield stress in dense slurries: Coal and other irregular particles, *Rheol. Acta*, *24*, 75–91.

Zlotnicki, J., G. Boudon, and J.-L. Le Mouel (1992), The volcanic activity of La Soufrière de Guadeloupe (Lesser Antilles): Structural and tectonic implications, *J. Volcanol. Geotherm. Res.*, *49*, 91–104.

M. Boichu, Department of Geography, University of Cambridge, Downing Place, Cambridge CB2 3EN, UK. (mb632@cam.ac.uk)

G. Boudon and B. Villemant, Institut de Physique du Globe de Paris, Équipe de Géologie des Systèmes Volcaniques, CNRS UMR 7154, 4 place Jussieu 75005 Paris, France.